Immobilization of molybdenum by alternative cementitious binders and synthetic C-S-H: An experimental and numerical study

Laura Diaz Caselles, Cédric Roosz, Julie Hot, Simon Blotevogel, Martin Cyr

Immobilization of molybdenum by alternative cementitious binders and synthetic C-S-H: an experimental and numerical study

Laura Diaz Caselles*, Cédric Roosz, Julie Hot, Simon Blotevogel, Martin Cyr

LMDC, INSA/UPS Génie Civil, 135 Avenue de Rangueil, 31077 Toulouse cedex 04 France.

*Corresponding author: diazcase@insa-toulouse.fr

Abstract

Excavation operations during construction produce millions of tons of soil sometimes with high leachable molybdenum (Mo) contents, that can lead to risks for both human health and the environment. It is therefore necessary to immobilize the Mo in excavated soils to reduce pollution and lower the costs of soil disposal. This paper studies the immobilization of Mo by three cementitious binders. To this end, one Ordinary Portland cement (OPC), one binder composed of 90% ground granulated blast furnace slag (GGBS) and 10% OPC, and one supersulfated GGBS binder were spiked with sodium molybdate at six different Mo concentrations from 0.005 wt% to 10 wt% before curing. In addition, to gain mechanistic insights, the capacity of synthetic calcium silicate hydrates (C-S-H) to immobilize Mo was studied. This study was completed by thermodynamic modeling to predict the immobilization of Mo at low Mo concentrations (<0.005 wt%). Paste leaching tests results showed that more than 74% of the initial Mo spike was immobilized by the three binders. The supersulfated GGBS binder consistently showed the highest retention levels (92.0 to 99.7%). The precipitation of powellite ($CaMoO_4$) was the dominant mechanism of Mo retention in all binders and most leaching solutions were oversaturated with respect to powellite. Also, in C-S-H syntheses, Mo was largely immobilized (>95%) by the coprecipitation of powellite. Thermodynamic modeling was in good agreement with measured values when the

equilibrium constant of powellite was modified to LogK=-7.2. This suggested that powellite is less stable in cementitious environments than would be expected from thermodynamic databases. Moreover, modeling showed that, for a solution at equilibrium with portlandite or C-S-H, the Mo concentration is limited to 1.7 mg/L by powellite precipitation. In contrast, for a solution saturated with respect to ettringite, the threshold concentration for powellite precipitation is 6.5 mg/L.

Keywords: Stabilization mechanisms; leaching; thermodynamic modeling; ground granulated blast furnace slag; powellite; contaminated soils

1. Introduction

Molybdenum (Mo) is an essential nutriment for plants and animals but it becomes toxic at high exposure levels (Erdman et al., 1978; Gupta, 1997; Van Gestel et al., 2012; Wenzel and Alloway, 2013). In France, excavated soils are classified into three categories following the European definitions (Directive 2008/98/EC, decision 2000/532/EC and decision 2001/573/EC) adopted by the French Ministerial decree on waste classification for disposal (Legifrance, 2014): (i) inert and non-hazardous, (ii) non-inert and non-hazardous or (iii) hazardous waste, depending on their leachable Mo concentrations (0.5, 10 and 30 mg_{Mo}/kg of dry soil, respectively). Excavation operations during construction of the subway project "Grand Paris Express" will produce millions of tons of excavated soil. Standardized leaching tests have shown that leachable Mo concentrations are higher than 3 mg_{Mo}/kg of dry soil (Cabrerizo et al., 2020), which is 6 times higher than the "inert and non-hazardous waste" limit set by the French Ministerial decree. Thus, it is desirable to immobilize Mo in excavated soils in order to reduce the amount of hazardous waste and lower the costs of soil disposal.

In soils, Mo is found as molybdate (MoO_4^{2-}) with the oxidation state +6 (Basta et al., 2005; Bourg and Loch, 1995; Plant et al., 2001). Bedrock of all types contains Mo in the mg/kg range, and some Mo based minerals have been identified (Smedley and Kinniburgh, 2017). The most common mineral is molybdenite (MoS_2), which is found in granite (Gupta, 1997). Mo can also be present in the environment as a result of anthropogenic activities (e.g. production of alloys in metallurgy, oil operations, industrial agriculture). For example, mineral sources of Mo such as ammonium molybdate ($(NH_4)_6Mo_7O_{24}\cdot 4H_2O$), sodium molybdate dihydrate ($Na_2MoO_4\cdot 2H_2O$) and sodium molybdate (Na_2MoO_4) are used as fertilizers to ensure against Mo deficiency (Wenzel and Alloway, 2013). During mineral weathering, Mo is released into the soil solution, where its mobility is controlled by adsorption on mineral and organic surfaces (Goldberg et al., 1996; Gustafsson and Tiberg, 2015; Marks et al., 2015; Wichard et al., 2009; Yang and Wang, 2021). Under certain conditions, this mobile Mo pool

62 is readily leached from soils and legal limits of Mo leaching are sometimes exceeded even in
63 unpolluted natural soils.

64 A common treatment of soils containing mobile heavy metals is the stabilization/solidification
65 (S/S) with ordinary Portland cement (OPC) and with other alternative cementitious binders
66 such as slag cements, pozzolanic cements and calcium aluminate cements (Chen et al.,
67 2021, 2009; Guo et al., 2017; Li et al., 2021; Spence and Shi, 2004; Wang et al., 2019,
68 2020). Kogbara and Al-Tabbaa, 2011 showed that leachable concentrations of several
69 heavy metals (Cd, Ni, Zn, Cu et Pb) decreased in contaminated soil after treatment with
70 slag-based binders. Wang et al., 2019 investigated the S/S of As and Pb in contaminated
71 soil by using calcinated clays. This study demonstrated that heavy metals leachability from
72 this soil was decreased by 96-98% after the reaction of calcined clays. Chen et al., 2021
73 showed that the S/S of a municipal waste containing predominantly mobile Pb was efficient
74 (about 89% of retention) by its treatment with calcium aluminate cement containing
75 phosphate additives.

76 Several mechanisms of heavy metal immobilization in cement-based materials have been
77 reported, including (i) redox reactions (Batchelor, 2006; Mancini et al., 2020), (ii)
78 precipitation and co-precipitation of poorly soluble species (Chen et al., 2021, 2009; Hills et
79 al., 1994), (iii) adsorption onto the surface of hydration products (Basta et al., 2005;
80 Grambow et al., 2020; Lange et al., 2020), and (iv) substitution and inclusion in the reaction
81 products (Berger, 2009; Chrysochoou and Dermatas, 2006; Goetz-Neunhoeffer and
82 Neubauer, 2006; Wang et al., 2020). Several studies have reported that powellite ($CaMoO_4$)
83 precipitation controls Mo solubility in Portland cement binders (Glasser, 1997; Kindness et
84 al., 1994; Minocha and Goyal, 2013). Other investigations have suggested a partial
85 immobilization of Mo during the formation of synthetic ettringite and monosulfoaluminate
86 (AFm) through the substitution of sulfate (SO_4^{2-}) by molybdate (MoO_4^{2-}) (Grambow et al.,
87 2020; Lange et al., 2020; Vollpracht and Brameshuber, 2016; Zhang and Reardon, 2003).
88 The similar tetrahedral structure of the sulfate and molybdate anions allows this substitution

even though molybdate (MoO_4^{2-}) is larger than the sulfate ion. Another study showed that MoO_4^{2-} can also replace Cl^- in AFm interlayers (Marty et al., 2018). At low Mo concentration levels, the adsorption onto the surface of amorphous hydration products such as calcium silicate hydrate (C-S-H) is a possible immobilization mechanism (Chen et al., 2009; Grambow et al., 2020; Lange et al., 2020; Park, 2000; Spence and Shi, 2004).

Some studies have addressed the mechanisms of Mo immobilization in OPC binders (Glasser, 1997; Kindness et al., 1994; Minocha and Goyal, 2013). However, there is no data available on the immobilization of Mo by alternative and more “environmentally friendly” binders and, thus, there is a need to better understand the interaction of Mo with cementitious binders in order to envisage treatment of Mo-contaminated soils. Therefore, the present study aims to (i) compare the capacity of alternative binders to immobilize Mo, (ii) study the immobilization of Mo by C-S-H, and (iii) contribute to the understanding of the mechanisms leading to Mo stabilization by comparing experimental data with thermodynamic models.

One OPC (referred to as CEM I) was used as the reference material, one binder composed of 90% ground granulated blast furnace slag (GGBS) and 10% OPC (referred to as 90-10) and one supersulfated GGBS cement (referred to as SSC), were selected so that their ability to chemically immobilize Mo could be studied. Before hydration, the binders were spiked with sodium molybdate at six different Mo concentration levels varying from 0.005 to 10 wt% (% by weight of anhydrous binder). After hydration, the mobility of Mo was evaluated by a leaching test. In a second step, C-S-H phases were synthesized in the presence of Mo in order to evaluate their contribution to the immobilization of Mo. To identify Mo stabilization mechanisms, all solid samples were analyzed using mineralogical and microscopic techniques. Mo and major element concentrations in leachates and in solutions after binder paste leaching tests and C-S-H syntheses were experimentally analyzed and

thermodynamically modeled to extrapolate experimental results to lower Mo concentrations (<8 mg/L).

2. Materials and methods

2.1. Materials

2.1.1. Molybdenum source

Sodium molybdate (Na_2MoO_4) purchased from Alfa Aesar (sodium molybdate anhydrous - Mo 46.2 wt%, purity >99.9%) was used to spike three different cementitious binders and for C-S-H syntheses with Mo. Using Na_2MoO_4 as a spike has the advantage of high water solubility (84 gNa_2MoO_4/100 ml at 25ºC) and contains Mo in the most common oxidation state, +6 (Vollpracht and Brameshuber, 2016).

2.1.2. Binders

The chemical and mineralogical compositions of the three anhydrous binders are listed in Table 1. The binders tested were:

- CEM I: Ordinary Portland cement, CEM I 52.5 N CE CP2 NF, referred to as “CEM I”. The main hydration products of this cement are portlandite (CH), calcium silicate hydrate (C-S-H) and ettringite (AFt).

- 90-10: Experimental binder composed of 90% ground granulated blast furnace slag (GGBS) and 10% OPC (the OPC designation refers to CEM I 52.5 N R CE CP2 NF), referred to as “90-10”. The addition of Portland cement to the slag is required to provide the necessary alkalinity to start the reaction of GGBS (Hewlett and Liska, 2019). This binder has been used in previous studies and showed good performance for immobilization of other anions such as sulfate (Diaz Caselles et al., 2020). The main hydration products in slag blended with clinker cements include C-(A)-S-H (with alumina replacing some silica), hydrotalcite (M_5AH_{13}) and other phases such as C_4AH_{13} (Chen

and Brouwers, 2007; Kolani et al., 2012) and AFt to a minor extent (Blotevogel et al., 2020).

- SSC: Supersulfated GGBS cement, in conformance with EN 15743. This cement is composed of about 70-90% GGBS, 10-20% calcium sulfate and 1-3% OPC. The main hydration products of this binder are AFt and C-(A)-S-H. Other phases such as M_5AH_{13} may also precipitate (Matschei et al., 2005).

Table 1 – Chemical and mineralogical compositions of anhydrous binders (% by weight). The GGBS(1) and OPC binders were used to fabricate the binder B2 (90-10). The GGBS(2) was used in the SSC cement. No crystallized phases were detected in GGBS due to their glassy structure.

		CEM I	90-10		GGBS(2)
			GGBS(1)	OPC	
Oxide composition	CaO	64.5	43.8	64.1	43.0
	SiO_2	20.2	37.4	21.9	36.0
	Al_2O_3	5.2	10.2	3.96	11.9
	Fe_2O_3	3.3	0.60	3.1	0.47
	MgO	0.80	6.4	1.3	7.0
	Mn_2O_3	ND	0.20	0.03	0.17
	Na_2O	0.28	0.21	0.15	0.34
	K_2O	0.76	0.28	0.74	0.45
	SO_3	3.0	0.10	3.4	0.10
	Cl^-	0.07	ND	ND	ND
Clinker composition	C_3A	8.6	-	8.0	-
	C_3S	60.3	-	53.7	-
	C_2S	12.6	-	22.4	-
	C_4AF	10.1	-	9.4	-
	$C\bar{S}$	5.1	-	5.8	-
	LOI	1.8	0	1.26	0

ND: Not determined

LOI: Loss on ignition, T=1000°C

2.1.3. Sample preparation and curing

Seven different pastes were cast for each binder type (a reference binder without Mo and six mixtures containing different initial Mo concentrations). All binder pastes were fabricated keeping a liquid to binder (L/B) ratio of 0.4 and following the recommendations of the European Standard EN 196-3. For spike binders, Na_2MoO_4 was first dissolved in the mixing water by adding six different levels of Mo: 0.005, 0.05, 0.1, 1, 5 and 10 wt% Mo, (% were calculated by weight of anhydrous binder) (50, 500, 1000, 10000, 50000 and 100000 mg_{Mo}/kg_{binder}, respectively). These concentrations were chosen to study the capacity of binders to immobilize Mo at different concentrations and to guarantee experimental Mo detection. Second, the binder was added to the Mo-solution. All pastes were cast into 6x12 cm hermetic cylinder recipients and the fresh mixture was vibrated for 30 s on a vibrating table in order to expel air bubbles. All samples were kept in the hermetic recipients and cured for 28 days at 20 °C in order to maintain a constant water content.

2.2. Methods

2.2.1. Leaching tests

Mo immobilization was evaluated by carrying out leaching tests in accordance with the European Standard NF EN 12457-2 as required by the French Ministerial decree on waste classification for disposal (Legifrance, 2014). This method evaluates leachable Mo and other leachable constituents in waste materials by a single-step batch procedure using distilled water (Buj et al., 2010; Diaz Caselles et al., 2020; Diotti et al., 2020; Helser and Cappuyns, 2021; Nikravan et al., 2020). Hardened binder samples were crushed to a particle size below 4 mm and placed in 1 L polypropylene bottles containing distilled water with a solid to liquid ratio (S/L) of 100 g/L. All bottles were shaken for 24 h in an end-over-end tumbler at 7 rpm. The solid residue was separated by vacuum filtration using a 0.45 µm filter membrane. After

filtration, pH was measured in the solutions, which were then acidified to 2 v% nitric acid (HNO_3). All solutions were stored at 4 ºC until chemical analyses were performed. Mo and major element concentrations were measured in the leachate solutions using Inductively Coupled Plasma Atomic Emission Spectrometry (ICP-OES) (Optima 7000 DV, by Perkin Elmer). Additionally, leachable sulfate concentrations were determined by ion chromatography (Dionex Ion Chromatography System ICS-3000). For this, the solutions were diluted by a factor of 100 using ultrapure water (18.2 MΩ.cm). Two solution samples were analyzed per formulation and arithmetic mean values are presented with a confidence interval of 95%. It should be noted that, in the first part, leached concentrations are expressed in $mg_{element}/kg_{binder}$ in order to compare leachable Mo concentrations with the thresholds presented by the French Ministerial decree on waste classification for disposal. In the second part, when experimental data and Mo stabilization mechanisms are discussed, the leached concentrations are presented in mg/L of eluates, because the solubility is controlled by solution concentration and not by the amount of solid.

2.2.2. Syntheses of C-S-H phases with Mo

All synthetic C-S-H phases were prepared under a nitrogen atmosphere using a glovebox in order to minimize carbonation. Synthetic C-S-H phases were prepared in accordance with the protocol presented by Roosz et al., 2016 by using lime (CaO), amorphous silica (SiO_2), a water to solid (W/S) ratio of 50 and a stoichiometric Ca/Si ratio of 1.6. W/S was set at 50 to ensure an amount of water in excess, which leads to a rapid dissolution of lime and silica in solution and thus, a rapid synthesis of C-S-H (Hewlett and Liska, 2019; Taylor, 1997). On the other hand, high Ca/Si ratio increases the positive surface charges of C-S-H, which increases the potential to immobilize anions (Grambow et al., 2020; Lange et al., 2020).

First, CaO was calcined in a furnace at 1000 °C for 8 h in order to ensure the absence of portlandite ($Ca(OH)_2$). Second, Na_2MoO_4 was dissolved in ultrapure water (18.2 MΩ.cm) in order to obtain five different Mo concentrations: 0, 0.25, 1, 2.5 and 5 wt% (% by weight of

199 $CaO+SiO_2$). These concentrations were chosen to study the capacity of C-S-H to immobilize
200 Mo at different concentrations and to guarantee experimental Mo detection. Then, 11.98 g of
201 CaO and 8.02 g of SiO_2 were added to the Mo-solution. Finally, all solutions were stored in
202 250 ml polypropylene bottles and shaken in an end-over-end tumbler at 7 rpm for 30 days.
203 The solid precipitate was separated by centrifugation and filtration using a vacuum device
204 and 0.22 µm membrane filters. C-S-H samples were stored under vacuum to prevent
205 carbonation. In the supernatant, pH was measured and then the solutions were acidified to
206 2 v% HNO_3 to analyze remaining element concentrations by ICP-OES.

207 *2.2.3. XRD analyses*

208 In order to identify Mo-bearing phases, mineralogical analyses were carried out on Mo-
209 spiked binder samples and in synthetic C-S-H phases using XRD analyses. All the samples
210 were crushed to a particle size below 80 µm. A Bruker D8 diffractometer in Bragg-Brentano
211 configuration with a copper radiation source (Cu Kα, λ=1.54 Å) was used. The anode voltage
212 was 40 kV, the electric current intensity was 40 mA. Angles from 2θ 5° to 70° were scanned
213 with a step size of 2θ 0.0203° and a total scan duration of 30 min. Rutile (TiO_2) was used as
214 an internal standard to normalize the peak intensities.

215 *2.2.4. Thermogravimetric and FT-IR analyses*

216 TGA was performed using two different devices: a Netzsch STA449-F3 and a TG2 by
217 Mettler Toledo. The heating rate was 10 ºC/min over the temperature range 40-1000 ºC.
218 Before TGA measurements, the synthetic C-S-H samples were humidified for two days in a
219 controlled nitrogen atmosphere using potassium sulfate (K_2SO_4). Then, humidified synthetic
220 C-S-H samples were dried in an oven at 40 ºC in order to remove the bulk water (Gaboreau
221 et al., 2020) and TGA was performed immediately after drying. On the same samples, FT-IR
222 was used to detect structural modifications on the Si-O bonds present in C-S-H samples,
223 using a Perkin Elmer UATR1 device with a diamond crystal. Data were collected over the
224 wavenumber range of 4000-600 cm^{-1}.

225 *2.2.5. Scanning electron microscope observations and EDS analyses (SEM/EDS)*

226 SEM observations were carried out on carbon-coated polished sections of hydrated binders
227 previously mounted in resin. The synthetic C-S-H phases were observed in powder form.
228 Two different scanning electron microscopes were used, a JEOL JSM-6380LV and a
229 JEOL JSM 7800, equipped with Rontec XFLASH 3001 and SDD X-Max 80 mm^2 Electron
230 dispersive spectroscopy (EDS) detectors, respectively. Images were obtained in both
231 secondary electron (SE) and backscattered electron (BSE) configuration, applying
232 magnifications between 100x and 10000x. EDS mapping and EDS punctual analyses were
233 also carried out to identify correlations between major elements and Mo.

234 *2.3. Thermodynamic modeling*

235 Mineral-solution equilibria were calculated using the PHREEQC code version 3.0 (Parkhurst
236 and Appelo, 2013). In this code, equilibria are modeled considering the extended Debye-
237 Hückel activity coefficient model and using the Debye-Hückel B-dot relation (Helgeson,
238 1969). Modeling provides information about the equilibrium state of the solution
239 (concentrations and activities of ionic and molecular species as well as the Saturation
240 Indices (SI) of reactants and products. This implies that kinetics of the chemical reactions
241 were not taken into account by this model.

242 In this study, thermodynamic calculations with PHREEQC were used to (i) calculate the
243 saturation index of powellite in the leachate solutions obtained from binder leaching tests,
244 and (ii) create a model of C-S-H syntheses in order to predict the precipitation of powellite at
245 low Mo concentrations (<8 mg/L), that were not accessible experimentally. In regard to the
246 saturation index (SI), SI>0 indicates that powellite can precipitate (oversaturation of solution
247 with respect to powellite), when SI<0 powellite dissolves (undersaturation of solution with
248 respect to powellite), and S=0 means equilibrium between powellite and the solution
249 (Goldberg, 2006; Zhu and Anderson, 2002). In the C-S-H model, three main constituents
250 were introduced into the model: (i) amorphous silica (SiO_2), (ii) lime (CaO) and (iii) sodium

molybdate (Na_2MoO_4). SiO_2 and CaO were introduced into the model at fixed concentrations used for the experimental syntheses, while Na_2MoO_4 was introduced into the model at different concentrations. Experimental and numerical data were compared in order to validate the model. Then, the precipitation of powellite was modeled at lower Mo concentrations (<8 mg/L) to establish threshold concentrations for powellite precipitation. This model was run taking three different conditions into account: (i) a solution saturated in C-S-H, (ii) a solution saturated in ettringite (AFt), (iii) a solution saturated in portlandite (CH). It should be noted that the phenomenon of adsorption of Mo onto the surface of C-S-H was not modeled.

The thermodynamic properties used in this work came from the Thermoddem database (version 1.10) (Blanc et al., 2012). The equilibrium constants (Log K) of powellite reported in literature are evolving from -7.02 to -8.51 (Essington, 1990), and values used in this work came from Essington, 1990, and Felmy et al., 1992 calculations. The dissolution reactions used in this model are presented in Table 2.

Table 2 – Dissolution reactions and related equilibrium constants (Log K) used for the thermodynamic modeling from Thermoddem database (Blanc et al., 2012). Data for powellite came from Essington, 1990[1], and Felmy et al., 1992[2].

Solid Phases	**Dissolution reactions used to calculate solubility products**	**Log K**
SiO_2(am)	$SiO_2 + 2.0H_2O = 1.0H_4SiO_4$	-2.70
C0.7SH	$Ca_{1.4}Si_2O_{5.9496}H_{1.0992}$:$1.378H_2O + 2.8H^+ + 0.6724H_2O = 1.4Ca^{2+} + 2H_4SiO_4$	17.73
C0.8SH	$Ca_{1.6}Si_2O_{6.1698}H_{1.1396}$:$1.6122H_2O + 3.2H^+ + 0.218H_2O = 1.6Ca^{2+} + 2H_4SiO_4$	21.80
C0.9SH	$Ca_{1.8}Si_2O_{6.4048}H_{1.2096}$:$1.7014H_2O + 3.6H^+ = 1.8Ca^{2+} + 2H_4SiO_4 + 0.1062H_2O$	25.45
C1.0SH	$Ca_{2.0}Si_2O_{6.6436}H_{1.2872}$:$1.7542H_2O + 4.0H^+ = 2.0Ca^{2+} + 2H_4SiO_4 + 0.3978H_2O$	29.464
C1.1SH	$Ca_{2.2}Si_2O_{6.8821}H_{1.3642}$:$1.867H_2O + 4.4H^+ = 2.2Ca^{2+} + 2H_4SiO_4 + 0.7491H_2O$	33.727

C1.2SH	$Ca_{2.4}Si_2O_{7.1203}H_{1.4406}$:2.0692$H_2O$ + 4.8H^+ = 2.400Ca^{2+} + 2H_4SiO_4 + 1.1895H_2O	37.938
C1.3SH	$Ca_{2.6}Si_2O_{7.3957}H_{1.5914}$:2.1702$H_2O$ + 5.2H^+ = 2.6Ca^{2+} + 2H_4SiO_4 + 1.5659H_2O	42.40
C1.4SH	$Ca_{2.8}Si_2O_{7.687}H_{1.774}$:2.2274$H_2O$ + 5.6H^+ = 2.8Ca^{2+} + 2H_4SiO_4 + 1.9144H_2O	46.93
C1.5SH	$Ca_{3.0}Si_2O_{7.9783}H_{1.9566}$:2.2848$H_2O$ + 6.0H^+ = 3.0Ca^{2+} + 2H_4SiO_4 + 2.2631H_2O	51.45
C1.6SH	$Ca_{3.2}Si_2O_{8.2682}H_{2.1364}$:2.3446$H_2O$ + 6.4H^+ = 3.2Ca^{2+} + 2H_4SiO_4 + 2.6128H_2O	55.94
Portlandite	$Ca(OH)_2$ + 2H^+ = 1Ca^{2+} + 2H_2O	22.81
Powellite[1]	$CaMoO_4$ = Ca^{2+} + MoO_4^{2-}	-8.05
Powellite[2]	$CaMoO_4$ = Ca^{2+} + MoO_4^{2-}	-7.92

3. Results

3.1. Leaching tests in Mo-spiked binders

Figure 1 presents the concentrations of Mo, Ca, sulfate and Na measured in eluates after paste leaching tests. Figure 1 shows the leached concentrations plotted against the concentration of the initial Mo spike using a linear scale. Figure 1(a) and (b) presents the same information on a logarithmic scale in order to emphasize the behavior of the elements at low initial Mo concentrations (<1 wt%). It should be noted that leached concentrations are expressed in both $mg_{element}/kg_{binder}$ and mg/L of eluates in order to compare leachable Mo concentrations with the French Ministerial decree (Legifrance, 2014) and for discussion of Mo stabilization mechanisms (solubility is controlled by solution concentration and not by the amount of solid). In addition, Table 3 displays the pH values of the eluates after paste leaching tests, the percentage of Mo retention calculated for each formulation and the calculated powellite Saturation Index (SI).

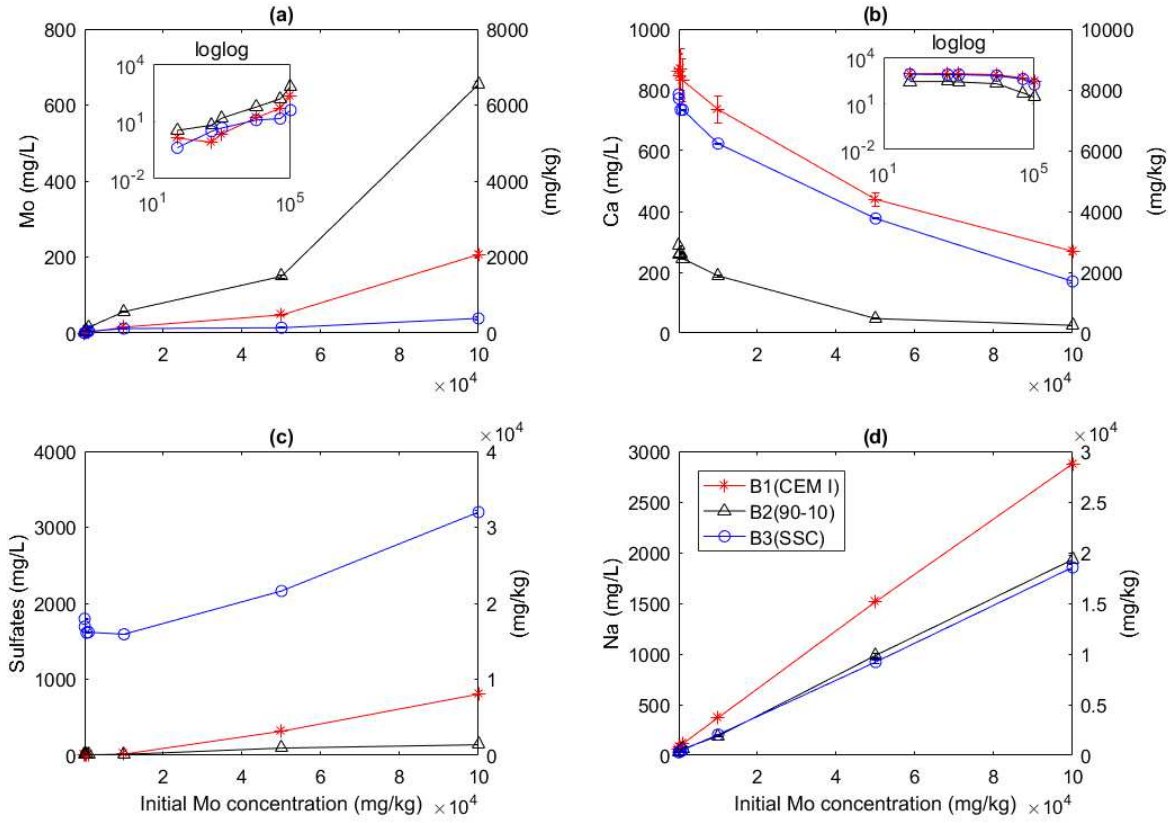

282

283 **Figure 1 –** Experimental leached element concentrations (expressed in mg/L on the y-axis at left and
284 in mg_{Mo}/kg_{binder} on the y-axis at right) plotted as a function of the initial Mo spike in the binders
285 expressed in mg_{Mo}/kg_{binder}. All values are related by lines for ease of reading and are presented in a
286 linear scale. Mo and Ca data are also plotted in logarithmic scale to analyze trends at low Mo
287 concentrations. **(a)** Molybdenum, **(b)** calcium, **(c)** sulfates, **(d)** sodium. Two solution samples were
288 analyzed per formulation and arithmetic mean values are presented with a confidence interval of 95%.

289 **Table 3** – Mo retention as a percentage in the three binders (B1, B2 and B3), pH values of eluates
290 after paste leaching of Mo-spiked binders and calculated powellite Saturation Index (SI). Each point is
291 the arithmetic average of two values.

Initial Mo concentration		B1 (CEM I)			B2 (90-10)			B3 (SSC)		
wt%	mg_{Mo}/kg_{binder}	pH	Mo retention (%)	SI	pH	Mo retention (%)	SI	pH	Mo retention (%)	SI

0	0	13.1	-	-	12.60	-	-	12.02	-	-
0.005	50	13.0	74.0	0.26	12.52	32.0	0.62	11.78	92.0	-0.34
0.05	500	13.1	98.4	-0.03	12.61	87.4	0.83	11.84	94.0	0.50
0.1	1,000	13.0	97.8	0.48	12.55	85.0	1.18	11.82	95.5	0.67
1	10,000	13.0	98.5	1.28	12.58	94.4	1.62	11.95	98.8	1.02
5	50,000	13.1	99.0	1.39	12.94	97.0	1.17	12.26	99.7	0.74
10	100,000	13.2	97.9	1.62	13.02	93.5	1.36	12.40	99.6	0.71

As presented in Figure 1, Mo concentrations in eluates increased with increasing initial Mo concentrations in all three binders. However, the concentrations in eluates were much lower than the initial Mo concentrations. Table 3 shows that, at high Mo concentrations (>0.1 wt%), more than 85% of Mo was immobilized by all binders. At the highest initial Mo concentration (10 wt%), leached Mo concentrations were 2070, 6550 and 390 mg_{Mo}/kg_{binder} for B1 (CEM I), B2 (90-10) and B3 (SSC), respectively. This corresponds to a Mo retention of 97.9, 93.5 and 99.6%. At low Mo concentrations (<0.1 wt%), relative Mo retentions were lower. For the lowest Mo concentration (0.005 wt%), leached Mo concentrations were 13, 34 and 4 mg_{Mo}/kg_{binder} for B1 (CEM I), B2 (90-10) and B3 (SSC), respectively. This corresponds to a Mo retention of 74, 32 and 92%. Thermodynamic calculations of the Saturation Index (SI) of powellite showed that almost all solutions were oversaturated with powellite except for the 0.05 wt% Mo solution in B1 (CEM I) and the 0.005 wt% Mo solution in B3 (SSC) (cf. Table 3). Oversaturation with powellite was generally higher in solutions with higher initial Mo concentrations. Also, oversaturation with powellite was slightly lower in B3 (SSC) (SI between 0.50 and 1.02) than in B1 (CEM I) and B2 (90-10) (SI between 0.26 and 1.62). Only two leaching solutions were not oversaturated with powellite: for B3 (SSC), the solution with the lowest Mo spike was undersaturated (SI=-0.34), and for B1 (CEM I), the solution with 0.05 wt% Mo spike was close to equilibrium (SI=-0.03).

3.2. XRD characterization of Mo-spiked binders

Figure 3 presents the XRD patterns of all the Mo-spiked binders, which are plotted for two angular ranges (2θ 17.5º-19º and 27º-30º) in order to zoom on the main powellite peaks (2θ 18°-19° and 2θ 28°-29°). Besides rutile (2θ 27°-28°), which was used as an internal standard, ettringite (2θ 17.5º-18º), portlandite (2θ 28º-29º), gypsum (2θ 29º-29.5º) and calcite (2θ 29º-30º) were identified. Powellite was detected in all binders that contained 5 and 10 wt% Mo. For binder B3 (SSC), a modification of the diffraction pattern in the range of powellite was observed at 1 wt% Mo, which is likely due to the minor presence of powellite. At Mo concentrations lower than 1 wt%, powellite was not detected.

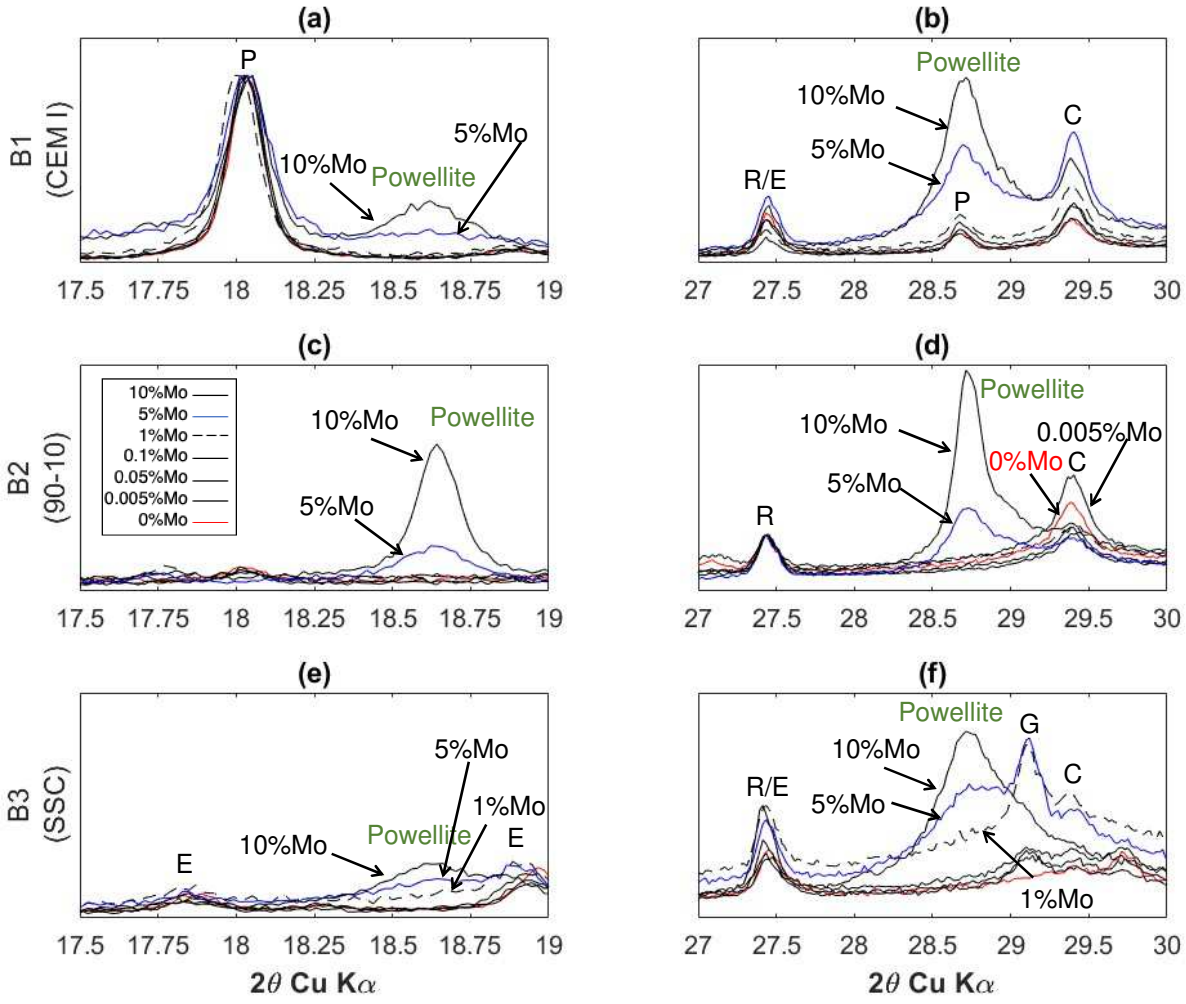

Figure 2 – XRD patterns obtained from Mo-spiked binders at 28 days of curing using rutile (TiO_2) as internal standard and plotted in the selected ranges 2θ 17.5º-19º **(left),** and 2θ 27º-30º **(right). (a)** and

(b) B1 (CEM I), **(c)** and **(d)** B2 (90-10), **(e)** and **(f)** B3 (SSC). *Legend:* ***P:*** *Portlandite,* ***R:*** *Rutile,* ***C:*** *Calcite,* ***E:*** *Ettringite,* ***G:*** *Gypsum.*

Figure 3 presents XRD patterns of all binders in the ranges corresponding to main ettringite peaks (2θ 8.8º-9.5º and 2θ 15º-17º). Ettringite was present in binders B1 (CEM I) and B3 (SSC) without Mo (0% Mo). Meanwhile, ettringite was not detected in the formulation B2 (90-10). It should be noted that no AFm phases were detected in the different samples. In formulation B1 (CEM I), no ettringite peaks were detected when the binder was spiked with Mo concentrations equal to or higher than 5 wt%. Meanwhile, in formulation B3 (SSC), ettringite peaks shifted toward lower angles with increasing spike Mo concentrations. Further details of this phenomenon will be addressed in the discussion section (cf. section 4.2).

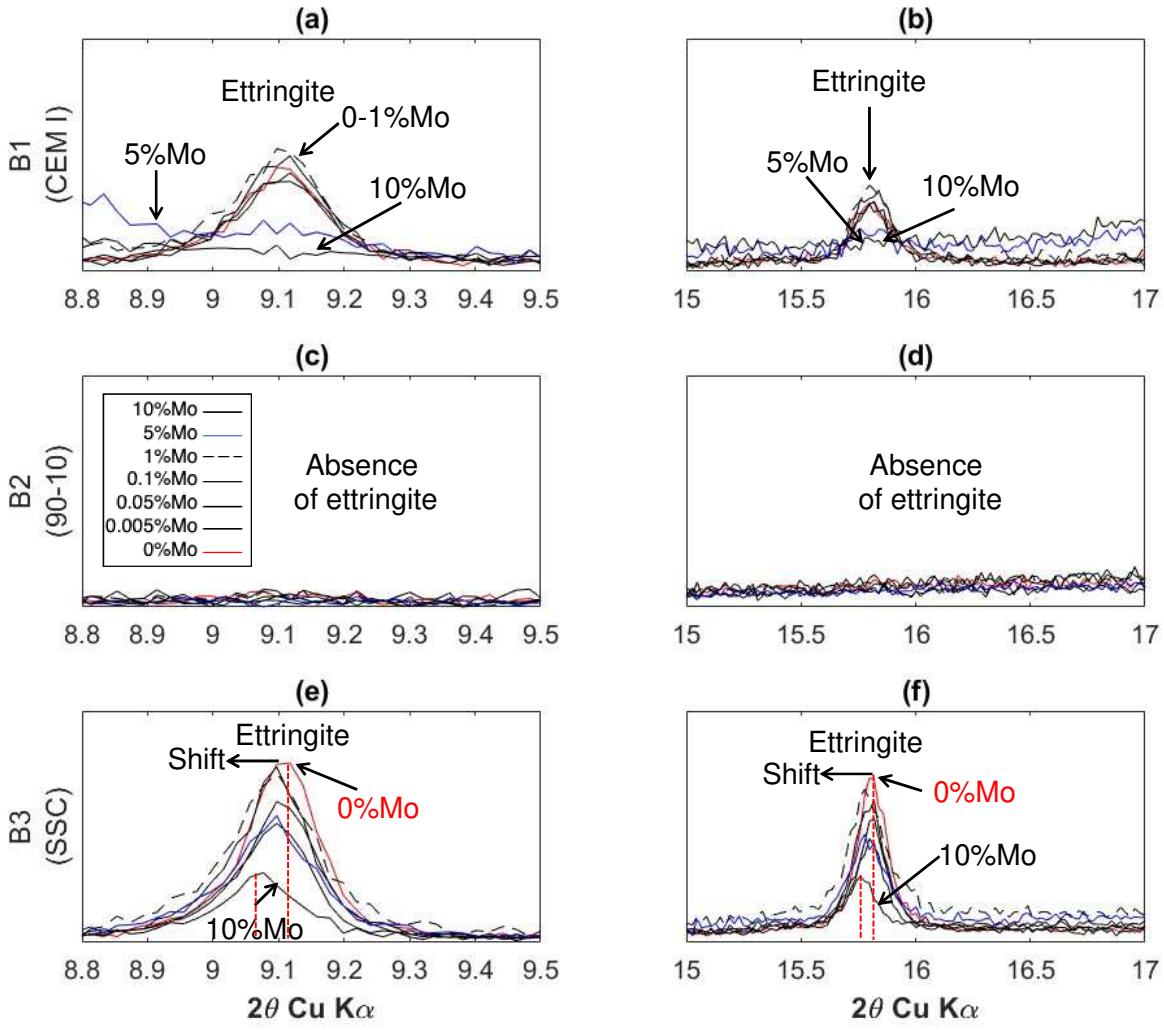

335 **Figure 3** – Superposed XRD patterns obtained from Mo-spiked binders at 28 days of curing using
336 rutile (TiO_2) as internal standard and plotted in the selected ranges 2θ 8.8º-9.5º **(left),** and 2θ 15º-17º
337 **(right). (a)** and **(b**) B1 (CEM I), **(c)** and **(d)** B2 (90-10), **(e)** and **(f)** B3 (SSC).

338 *3.3. Characterization of synthetic C-S-H phases in presence of Mo*

339 *3.3.1. XRD analyses of synthetic C-S-H phases*

340 Figure 4(a) presents the XRD patterns of all synthetic C-S-H samples in the range 2θ 5º-70º.
341 All patterns showed several characteristic peaks of rutile (TiO_2), which was used as an
342 internal standard. The C-S-H peak between 2θ 5º and 10º shifted slightly in position for the
343 C-S-H phase with 0.25 wt% Mo. Otherwise, the C-S-H peaks had identical position and
344 relative intensity for all samples. Moreover, powellite ($CaMoO_4$) was identified in all Mo-
345 spiked synthetic C-S-H samples and the relative intensity of powellite peaks increased with
346 increasing Mo concentrations (for ease of identification, color was added to powellite peaks).
347 Figure 4(b) and Figure 4(c) present zooms on the powellite peaks in the ranges 2θ 27º-32º
348 and 2θ 57º-60º, respectively. All diffraction patterns were normalized to the rutile peak at 2θ
349 27.4º.

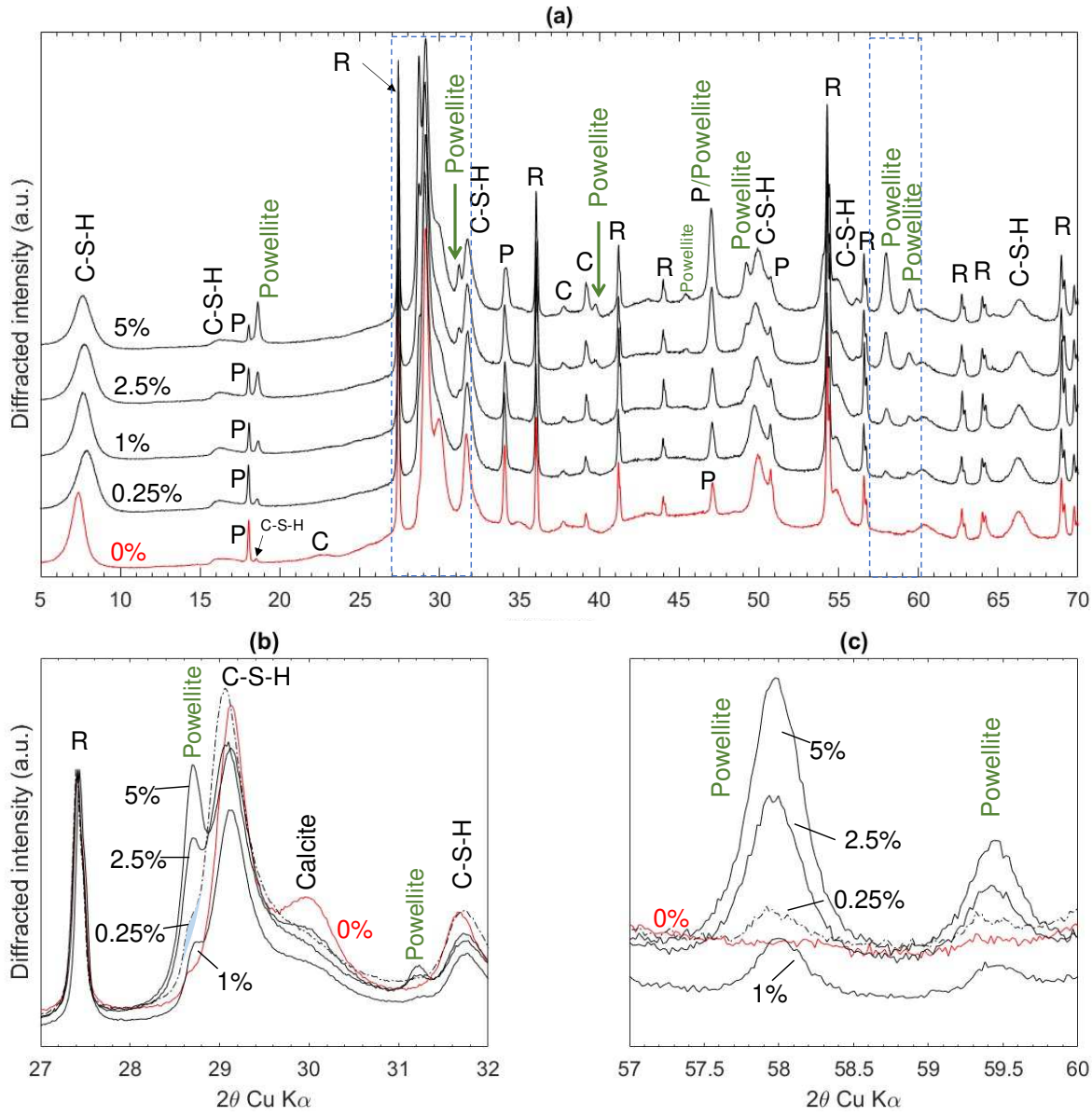

Figure 4 – XRD patterns of synthetic C-S-H with and without Mo using 10 wt% rutile (TiO_2) as internal standard. **(a)** range 2θ 5º-70º, **(b)** superposed patterns in 2θ 27º-32º, **(c)** superposed patterns in 2θ 57º-60º. Percentages in (b) and (c) refer to initial Mo concentrations given in % by weight (wt%). *Legend:* ***P:*** *Portlandite,* ***R:*** *Rutile.*

3.3.2. TGA analyses of synthetic C-S-H phases

Figure 5(a) and (b) present the TGA analyses carried out on synthetic C-S-H samples. In Figure 5(a), the weight loss between 100 °C and 200 ºC was attributed to the dehydration of C-S-H (Scrivener et al., 2015). The second temperature range of weight loss between

350 °C and 500 ºC was attributed to the dehydration of portlandite (CH), which was likely present due to the hydration of CaO. A third weight loss range between 600 °C and 800 ºC was mainly associated with the presence of carbonates (mono- or hemicarbonates and calcite) (Scrivener et al., 2015). This reflects the slight carbonation of synthetic C-S-H phases during their preparation. Figure 5(b) shows that the overall weight loss of synthetic C-S-H phases tended to decrease with increasing Mo concentration used in the syntheses of C-S-H. The total weight losses calculated from Figure 5(b) were: 21.3%, 21.5%, 19.5%, 19.8% and 18.6% for C-S-H with 0% Mo, 0.25 wt% Mo, 1 wt% Mo, 2.5 wt% Mo and 5 wt% Mo, respectively. This indicates a difference of loss of about 2.7% between the sample without Mo and the sample with the highest Mo concentration. However, no significant shifts in the temperature range of C-S-H dehydration were observed.

3.3.3 FT-IR analyses of synthetic C-S-H phases

Figure 5(c) and (d) show FT-IR spectra of the C-S-H phases. All spectra were normalized to the minimum value of each spectrum. In Figure 5(d), the spectra of sodium molybdate (Na_2MoO_4) and powellite ($CaMoO_4$) were also plotted in order to compare the position of the bands corresponding to the Mo-O group. The powellite spectrum was taken from the RRUFF ID R050355.2 database (Ponta et al., 2015).

As observed in Figure 5(c), FT-IR spectra showed the same absorption bands with some differences in their relative intensities. The main absorption bands and corresponding assignments were: 3600-3100 cm^{-1} (OH stretching), 1700-1600 $cm^{-1}$and 1600-1100 cm^{-1} (C-O stretching and O-H deformation), 1090-1050 cm^{-1} (asymmetric vibration of Si-O), 900 cm^{-1} (asymmetric vibration of Si-OH), and 795 cm^{-1} (symmetric vibration of Si-O) (Beganskienė et al., 2004). Similar positions and shapes of the main Si-O vibrations and the absence of supplementary bands indicate that the structure of the C-S-H phases was not modified by the presence of Mo.

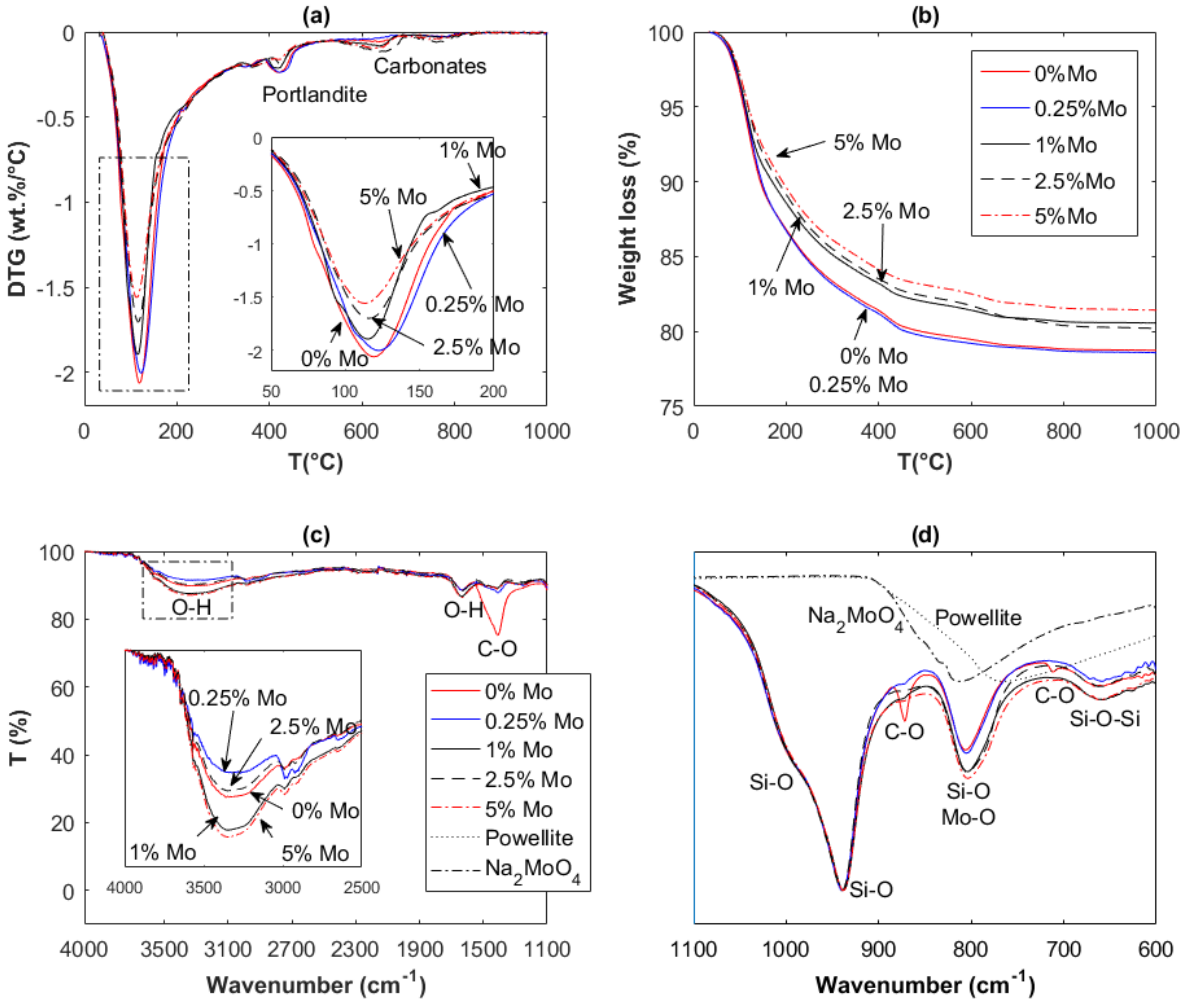

Figure 5 – Thermogravimetric (TGA) and FT-IR analyses of synthetic C-S-H phases. **(a)** Differential thermogravimetry (DTG) data of weight loss given in wt%/ºC, **(b)** weight loss given in percentage. All data were plotted as a function of temperature from 0 ºC to 1000 ºC (heating rate 10ºC/min), **(c)** FT-IR spectra were plotted in the 4000-1100 cm^{-1} range, and **(d)** in the 1100-600 cm^{-1} range.

3.3.3. SEM/EDS observations on synthetic C-S-H phases

Figure 6 shows the SE images obtained from synthetic C-S-H phases and the corresponding distribution of Ca/Si atomic ratios determined by EDS punctual analyses. The SEM images show the presence of several bright spots on the C-S-H surface when Mo was added to the solution. The amount and intensity of the bright spots increased with increasing concentration of Mo and EDS spectra on these spots confirmed the presence of Mo (Figure 6 middle). In the synthetic C-S-H with no Mo, EDS punctual analyses show that the average

value of Ca/Si atomic ratio was 1.62 (cf. Figure 6(a) at right). Figure 6(b) to Figure 6(e) show the same data for the synthetic C-S-H phases containing Mo from 0.25 to 5 wt% Mo. It can be observed that the average value of Ca/Si atomic ratio increased from 1.62 to about 1.68 when Mo was added to the solution (except for 2.5 wt% Mo, where the Ca/Si ratio was about 1.71). This was mostly attributed to the coprecipitation of powellite, which increased the amount of Ca in the solid.

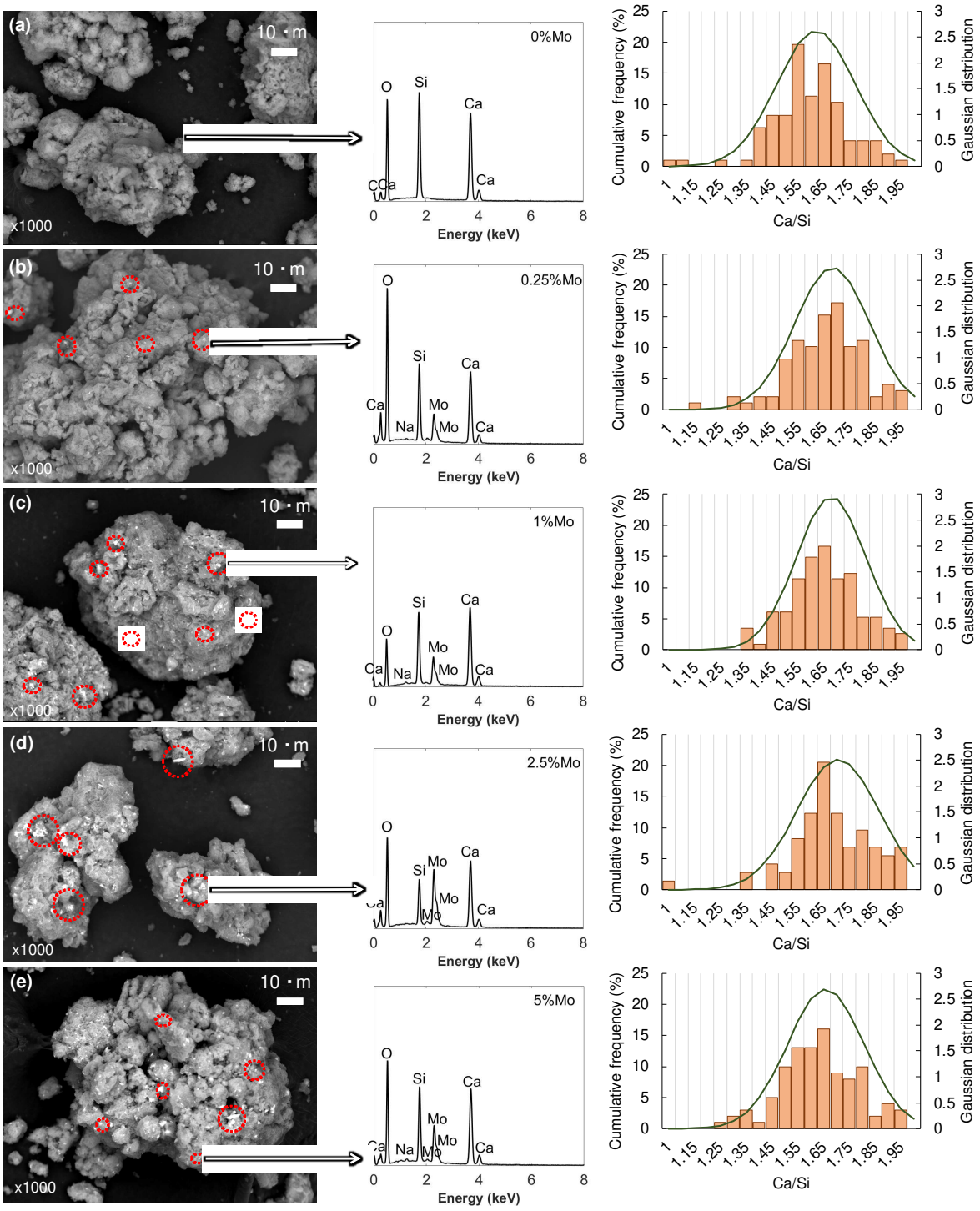

405

406 **Figure 6** - SEM/EDS analyses of synthetic C-S-H phases. **Left:** SE images, **Middle:** EDS spectra,
407 **Right:** Histograms of the Ca/Si ratios obtained from EDS punctual analyses. **(a)** 0 wt% Mo, **(b)**
408 0.25 wt% Mo, **(c)** 1 wt% Mo, **(d)** 2.5 wt% Mo, and **(e)** 5 wt% Mo.

409 Figure 7 presents mixing diagrams established from EDS analyses. Figure 7(f) shows the
410 expected regions for the different endmembers (C-S-H and Powellite). For the synthetic C-S-

H phase without Mo, the Si/Ca ratio varied from 0.5 to 0.7 (Ca/Si ratio from 2 to 1.4, respectively (cf. Figure 7(a)). In Figure 7 (b-e), representing the C-S-H sample containing Mo, the Si/Ca atomic ratios were similar to those of the sample without Mo addition. However, with increasing Mo content, an increasing number of measurements fall onto the mixing line of C-S-H and powellite.

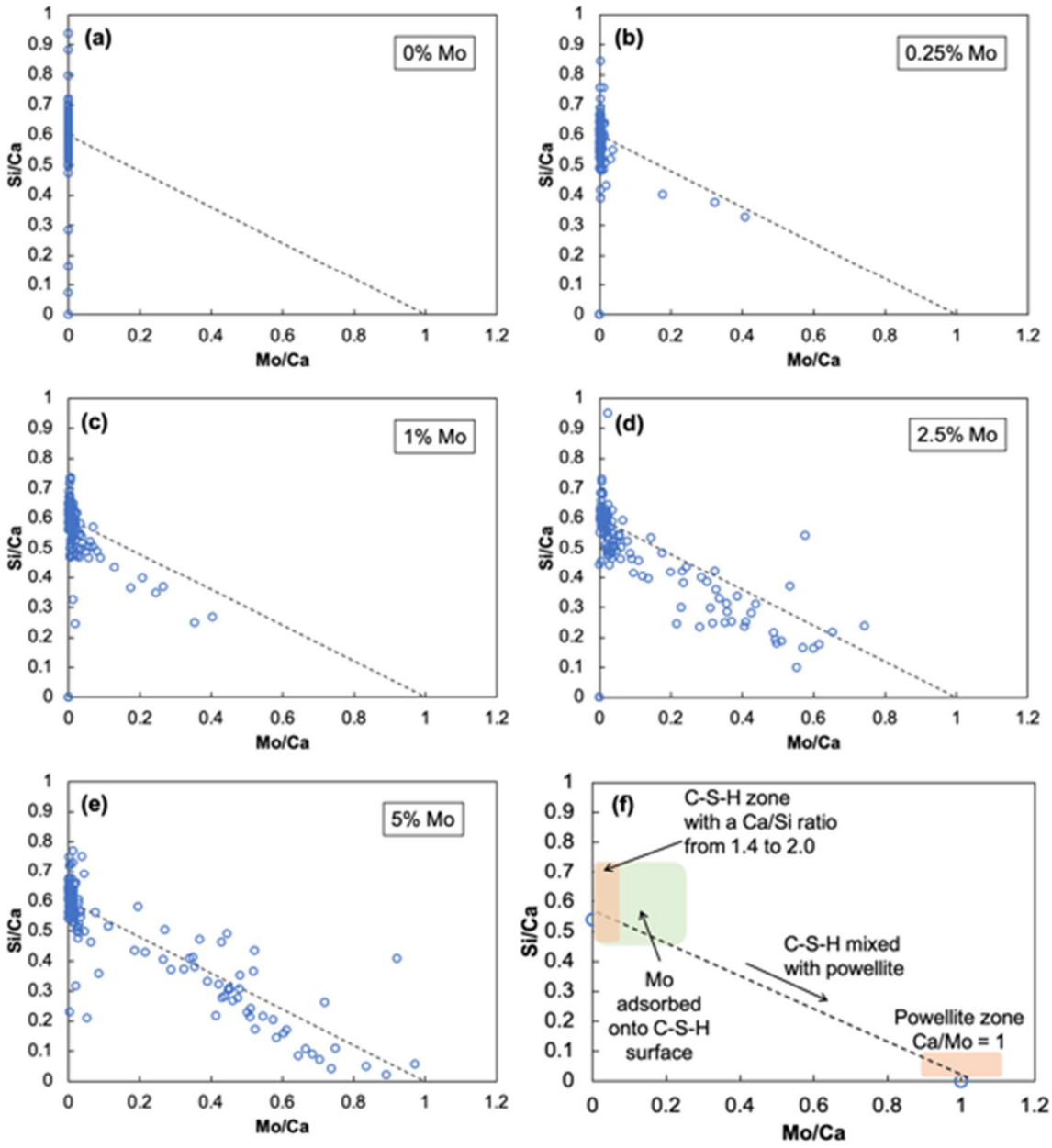

Figure 7 – Mixing diagram of Si/Ca vs. Mo/Ca atomic ratios from EDS punctual analyses for all synthetic C-S-H phases. The dotted line corresponds to the mixing line between C-S-H and powellite.

Each diagram presents results for one initial Mo concentration **(a)** 0% Mo, **(b)** 0.25% Mo, **(c)** 1% Mo, **(d)** 2.5% Mo, **(e)** 5% Mo. (Percentages by weight), and **(f)** interpretation of the chart, in which the green zone is placed only as a guide.

3.3.4. Mo concentration solution after C-S-H filtration: experimental and modeled element concentration remaining in solution

Figure 8 compares the modeled and experimental Mo, Si Ca, and Na concentrations in solution together with pH values obtained after C-S-H syntheses. Concentrations presented on the y-axis are given in mg/L and they are plotted against the initial Mo concentration used in syntheses expressed in % by weight of initial solid (initial solid = 20 g of $CaO+SiO_2$, Ca/Si of 1.6 and with a water to solid (W/S) ratio of 50). Experimental data are represented by circles while modeled values are given by lines.

Mo concentrations measured in solution decreased by more than one order of magnitude after the C-S-H syntheses. This corresponds to a Mo retention in the solid phase of 95 to 99%. Na concentrations increased linearly with increasing initial Mo concentrations, due to the use of sodium molybdate (Na_2MoO_4) as Mo source (cf. Figure 8(c)). In solutions with no added Mo, the remaining Ca (984 mg/L) and Si (about 12.5 mg/L) were the highest. In solutions with Mo, Ca concentrations decreased with the addition of Mo and reached 579 mg/L at the highest Mo concentration (5 wt%) (cf. Figure 8(b)), In contrast, Si concentrations remained relatively constant with Mo addition, close to 1 mg/L (cf. Figure 8(b)). In addition, pH values of these samples remained relatively stable between 12.5 and 12.8 (cf. Figure 8(e)).

Overall, modeled solution concentrations were close to experimental data. In particular, Ca and Si concentrations in equilibrated solutions were well represented. In a first model using the thermodynamic data presented in Table 2, it was observed that, even though variations in Mo concentrations were well reproduced, the calculated concentrations were 10 times lower than the experimental values (dotted line in Figure 8(a)). A second model was created

446 by varying the equilibrium constant of powellite in an attempt to approach measured Mo
447 concentrations (solid line in Figure 8(a)). This modification showed no impact on the other
448 calculated element concentrations. The Mo concentrations in solution were well represented
449 when an equilibrium constant of LogK = -7.2 was used for the formation of powellite.
450 Modeled powellite precipitation evolved linearly from 0 (in the Mo-free sample) to 416.5 mg
451 (in the sample with the highest initial Mo concentration of 5 wt%). The amount of precipitated
452 powellite in the most Mo spiked sample decreased from 416.5 mg to 415.0 mg, which can
453 be considered as negligible. The calculated pH values were slightly lower than experimental
454 values. The quantity of C-S-H in equilibrium with calculated solutions remained stable
455 around 4.4 g for all equilibrated samples (200 mL of initial solution).

456

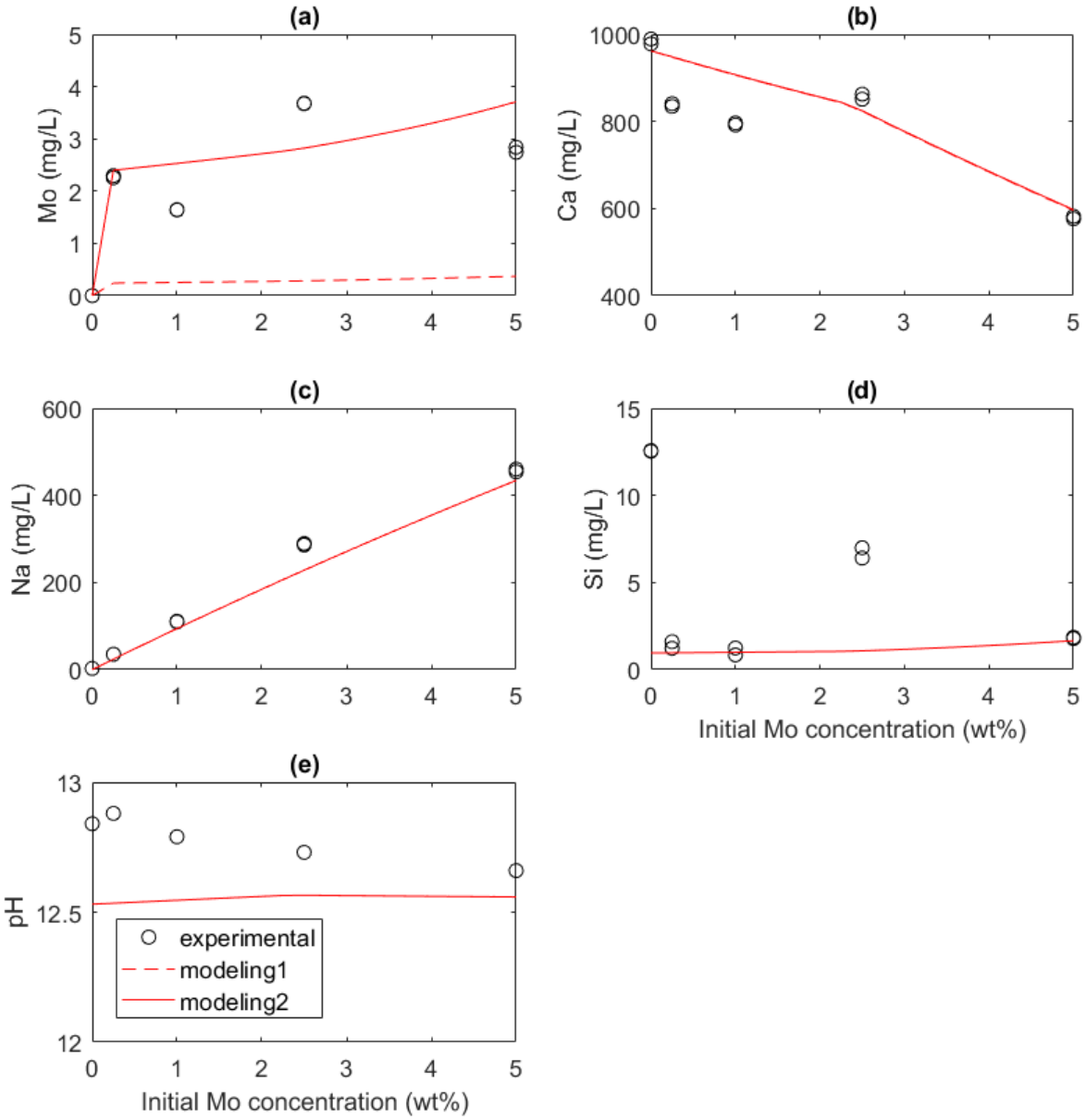

Figure 8 – Experimental and numerical data of element concentrations and pH values from the filtered solution after the syntheses of C-S-H with Mo. Concentrations are given in mg/L on the y-axis and plotted against initial Mo concentrations in % by weight of solid. Solid =20 g of $CaO+SiO_2$. **Circles:** experimental data. **Lines:** modeling. **(a)** molybdenum, **(b)** calcium, **(c)** sodium, **(d)** silicon, and **(e)** pH values.

4. Discussion

4.1. Capacity of alternative binders to immobilize Mo

Overall, all three binders showed the ability to immobilize Mo (cf. Table 3). Among the three binders, the supersulfated GGBS binder B3 (SSC) consistently showed the highest relative retention levels of Mo (from 92.0 to 99.6% of Mo retention) over the whole range of Mo concentrations tested. It was followed by the ordinary Portland cement B1 (CEM I) with Mo retention levels from 74 to 98% and the binder B2 (90-10) composed of 90% GGBS and 10% OPC with Mo retention levels from 32 to 94%. For the lowest spike Mo concentration (50 mg_{Mo}/kg_{binder}), binders B1 (CEM I) and B3 (SSC) presented leachable Mo concentrations of 13 and 4 mg_{Mo}/kg_{binder}, respectively. This reduction in leachable Mo would allow the transformation of an initially "hazardous waste" to "non-inert and non-hazardous waste". These binders present potential to efficiently immobilize Mo. Since this study was limited to model systems, further data on more complex real-world applications are needed (e.g. Mo-contaminated soils or waste material). Under these conditions, there might be additional effects due to the presence of organic matter, ion competition and other reactive surfaces.

Among the three binders studied, only the OPC has already been reported to immobilize Mo. Kindness et al., 1994 studied the immobilization of Mo in an Mo-spiked OPC and showed that leachable Mo concentration was 40 times lower than initial Mo concentration after 12 days of curing. Similarly, Minocha and Goyal, 2013, studied the immobilization of Mo in an OPC spiked with different Na_2MoO_4 concentrations. They showed that samples spiked with Mo at 1000, 1500 and 2000 ppm ($mg/kg_{solution}$) retained about 99% of Mo, in agreement with the retention values obtained in the present study.

4.2. Mechanisms of Mo retention in alternative binders

XRD analyses performed in the Mo spiked binders showed the presence of powellite at Mo concentrations ≥5 wt% (cf. Figure 2). This suggests that precipitation of powellite controls the Mo solubility at high initial Mo concentrations, in all three binders. The immobilization of Mo by OPC has already been reported and was explained by the precipitation of powellite

491 and the precipitation of an Mo-AFm phase (Kindness et al., 1994; Minocha and Goyal,
492 2013).

493 At lower Mo concentrations (≤1 wt%), powellite was not identified - probably because the
494 detection limits of the XRD analyses are relatively high. However, almost all solutions were
495 slightly oversaturated with powellite. This suggests that powellite is the controlling phase of
496 Mo mobility, even in samples where no powellite was detected by XRD. Powellite
497 precipitation was predominantly controlled by Ca availability. pH values may have an indirect
498 effect by modifying the stability of other Ca-bearing phases (e.g. C-S-H, ettringite,
499 portlandite). Furthermore, the slight oversaturation indicates that the stability of powellite in
500 cementitious systems is not exactly represented by the equilibrium equation. In fact, it
501 appears to be somewhat less stable, which was confirmed by the modeling of C-S-H and will
502 be discussed in section 4.4.2. The reduced leachate concentrations of Ca in the presence of
503 Mo (cf. Figure 1) further support powellite precipitation. In binder B2 (90-10), with the lowest
504 leached Ca concentrations, the deficit of available Ca probably limited powellite precipitation,
505 thus explaining the lower Mo retention rates. Similar oversaturation of leachates from B1
506 (CEM I) and B2 (90-10) support this mechanism. This illustrates the need for a sufficient Ca
507 supply if Mo is to be immobilized efficiently.

508 In binder B3 (SSC) the powellite SI values calculated in solution were systematically lower at
509 equal spike concentration than in B1 (CEM I) and B2 (90-10) (cf. Table 3). At the lowest
510 spiked Mo concentration, the solution was even undersaturated with powellite. This suggests
511 that the reaction controlling Mo mobility in B3 is slightly different from that in B1 and B2. This
512 may be due to a supplementary Mo immobilization mechanism such as adsorption,
513 substitution and inclusion, on which pH probably has a more important effect than in
514 powellite precipitation (Lange et al., 2020; Mancini et al., 2020; Minocha and Goyal, 2013;
515 Vollpracht and Brameshuber, 2016; Zhang and Reardon, 2003). Several studies have
516 suggested that Mo could be partially immobilized by sulfate-bearing phases, such as
517 ettringite. For example, Vollpracht and Brameshuber, 2016, studied the leaching of Mo in

518 several Portland cements during hydration. After pore solution extractions, they found that
519 molybdate concentrations followed a trend opposite to that of ettringite formation. Therefore,
520 the authors pointed out that molybdate may have partially replaced sulfate in ettringite.
521 Similarly, Zhang and Reardon, 2003, studied the immobilization of Mo, Cr, B and Se by
522 incorporation into ettringite. They showed that Mo was partially immobilized during ettringite
523 precipitation as Mo concentrations decreased from 10 ppm to 4 ppm.

524 Ettringite was present in B1 (CEM I) and B3 (SSC) binder samples. In both systems, sulfate
525 concentrations increased in solution with increasing Mo-spike concentrations. This would be
526 in line with a partial substitution of sulfate by molybdate in ettringite. In fact, XRD analyses
527 obtained from the binder B3 (SSC) showed that ettringite (a major hydrate of this binder)
528 was structurally modified at high Mo levels (≥1 wt%~10000 mg_{Mo}/kg_{binder}). The peak of
529 ettringite situated between 2θ 9º and 9.5º shifted toward lower angles, which implies an
530 increase in the d-spacing. According to the literature, the bond length of Mo-O is about
531 1.76 Å, which is around 1.2 times that of sulfate (~1.49 Å) (Vollpracht and Brameshuber,
532 2016; Zhang and Reardon, 2003). These observations are in line with a possible substitution
533 of sulfate by molybdate. As shifts in ettringite diffraction patterns were only observed in
534 binder B3 (SSC), this supplementary mechanism might explain the slight undersaturation of
535 the solution with respect to powellite at the lowest Mo spike.

536 For B1 (CEM I), the peaks of ettringite were identified in all the patterns except for the two
537 highest concentrations of Mo, in which the peaks of ettringite disappeared, probably
538 because of the high amount of Na in the solution. Na concentrations in solution mainly came
539 from the use of Na-molybdate as a spike. Several studies have shown that the presence of
540 high Na or K content inhibits the formation of ettringite (Brown and Bothe, 1993; Glasser,
541 2004), which may favor the precipitation of other phases, such as powellite. This
542 destabilization of ettringite likely explains the increased presence of sulfate in the eluates of
543 B1 (CEM I) at the highest initial Mo spike concentration.

544 *4.3. Syntheses of C-S-H in the presence of Mo: coprecipitation of powellite*

Calcium silicate hydrate (C-S-H) is the main hydration product of cementitious materials. In fact, all of the three binders studied in this paper produce C-S-H in different proportions during hydration. According to the literature, C-S-H allows the physical adsorption of heavy metals onto their surface (Glasser, 1997; Grambow et al., 2020; Lange et al., 2020; Park, 2000). In addition, C-S-H may compete with powellite for Ca ions in solution, so the immobilization of Mo during C-S-H formation was studied to advance the understanding of Mo retention mechanisms.

In all C-S-H syntheses, Mo was largely immobilized (>95%) over the whole range of Mo concentrations studied (0.25, 1, 2.5 and 5 wt% Mo). Again, the main immobilization mechanism appeared to be the precipitation of powellite, which was detected by XRD. SEM/EDS analyses showed the mixing of C-S-H and powellite with increasing initial Mo concentrations. The presence of powellite in C-S-H syntheses was in line with the slight decrease in Ca concentration in the filtered solution after C-S-H syntheses, while Mo concentration in the solid fraction increased. Moreover, all XRD patterns showed the presence of portlandite in all C-S-H samples, indicating that Ca was available in excess.

On the other hand, the structure of the C-S-H phases was not modified by the presence of Mo. In fact, XRD patterns were almost identical for all the synthetic phases. In addition, FT-IR spectra showed that the main Si-O vibrations were comparable in wavenumber and intensity for all the C-S-H phases. However, the band between 850 and 750 cm^{-1} increased in relative intensity with increasing Mo concentration. As no further Si-O bonds were present with increasing Mo concentration, this was likely due to the appearance of the Mo-O band associated with the precipitation of powellite (cf. Figure 5) (Ponta et al., 2015). Besides, the temperature range for dehydration during TGA was identical in all the C-S-H samples for all Mo concentrations. The small decrease in weight loss for samples with high initial Mo content was likely due to the dilution for C-S-H with powellite. These observations suggest that Mo was not included into the C-S-H structure and that there was no significant competition for Ca between powellite and C-S-H.

572 ### *4.4. Modeling of the precipitation of powellite*

573

574 #### *4.4.1. Experimental vs modeling of C-S-H in contact with Mo*

575 Predicted phase precipitation and solution concentrations values were well in line with
576 solution chemistry and mineralogical analyses. This implies that, by taking only the
577 precipitation of C-S-H and powellite into account, the main processes are represented. Other
578 processes, such as the adsorption of Mo onto the surface of C-S-H, cannot be excluded but
579 were not significant in this study. In fact, Lange et al., 2020 and Grambow et al., 2020
580 studied the adsorption of Mo by C-S-H phases. Both studies showed a strong retention of
581 Mo (in the form of molybdate) by synthetic C-S-H phases having Ca/Si ratios between 0.9
582 and 1.4. Lange et al., 2020, indicated that molybdate uptake by C-S-H can be explained by
583 the electrostatic sorption of Mo. However, both studies used much smaller Mo contents in
584 solution in order to avoid supersaturation of the solution with respect to powellite (initial
585 molybdate concentrations between $5x10^{-6}$ and $1x10^{-7}$ mol/L).

586 Mo concentrations in solution were correctly modeled only if the equilibrium constant (Log K)
587 was modified to -7.2 (-8.05 by Essington, 1990 and -7.92 by Felmy et al., 1992), bringing the
588 leaching solutions closer to equilibrium. This suggests that, in a cementitious environment,
589 powellite is less stable than predicted from the equation in Table 2. This is supported by the
590 oversaturation of solution leached from binders in Table 3. The proposed modification of the
591 equilibrium constant (Log K) was in the highly variable range of published values (-7.02 to -
592 8.51). This variability was previously attributed to the high dependence of experimental
593 values on the stability of Mo-rich aqueous species (Essington, 1990). In cementitious system
594 with many dissolved ions, the formation of aqueous Mo species other than MoO_4^{2-} (that are
595 not contained in the database) is possible.

596 #### *4.4.2. Modeling of the precipitation of powellite at low Mo concentrations*

597 Simulations were also carried out using Mo concentrations lower than 8 mg/L in order to
598 establish threshold values for the precipitation of powellite at low Mo concentrations that
599 were not tested experimentally (the equilibrium constant used for powellite was Log K=-7.2).
600 Because the stability of powellite depends only on the activity of Ca and Mo in solution (cf.
601 Table 2), the Ca activity and the pH in solution were fixed by the equilibrium with C-S-H,
602 ettringite (AFt) or portlandite (CH). Thus, this model gives the maximum values of dissolved
603 Mo in cementitious environments, controlled by these three phases.

604 Figure 9 presents the Mo concentrations and the evolution of the precipitation of powellite
605 calculated for the three different solutions. All data are expressed in mg/L and were plotted
606 as a function of the initial Mo concentration. As shown in Figure 9, Mo concentrations in
607 solution increased progressively up to the Mo concentration of 1.7 mg/L ($1.7x10^{-5}$ mol/L) and
608 1.8 mg/L ($1.9x10^{-5}$ mol/L) for a solution saturated with respect to C-S-H and CH. From these
609 concentrations, powellite started to precipitate. Addition of Mo beyond these points only
610 increased the powellite formation, not Mo concentration in solution. This Mo threshold
611 concentration was below 2 mg/L, which, considering a solid to liquid (S/L) ratio of 1/10 in
612 accordance with the European Standard NF EN 12457-2, would translate into leached Mo
613 concentrations of 20 mg/kg of dry mass, which is below the legal threshold of 30 mg/kg of
614 dry mass established for the “hazardous” waste category. Any Mo concentration can be
615 immobilized to this solution concentration by powellite precipitation in solutions that are
616 controlled by CH or C-S-H. However, these values are still well above the limit drinking
617 water concentration presented by the WHO (0.07 mg/L) (World Health Organization, 2004).
618 To reach even lower leachable Mo concentrations, the solution concentration of Ca would
619 need to be further increased (e.g. by adding an even more soluble Ca mineral). These
620 results show that any amount of Mo can be immobilized below legal limits by cementitious
621 binders, if the Ca availability is properly managed.

622 On the other hand, when the solution was saturated with respect to AFt, Mo concentrations
623 in solution increased, up to 6.5 mg/L ($7x10^{-5}$ mol/L), where powellite precipitation started.

When the Mo was added into solution beyond this point, the Mo concentration still slightly increased. This is likely due to an increase in pH due to the addition of Na_2MoO_4 to the model. In fact, AFt becomes more stable at higher pH values, and therefore, the Ca concentration in solution decreases, which increases the threshold Mo concentration for powellite precipitation. Therefore, the Mo retention by powellite precipitation is not sufficient to reach legal limits in solutions that are controlled by AFt. Nevertheless, the binder B3 (SSC) with the lowest pH and highest AFt contents showed the best Mo retention. This underlines that, in binder B3 (SSC), retention mechanisms other than powellite precipitation were at play at least at low Mo concentrations.

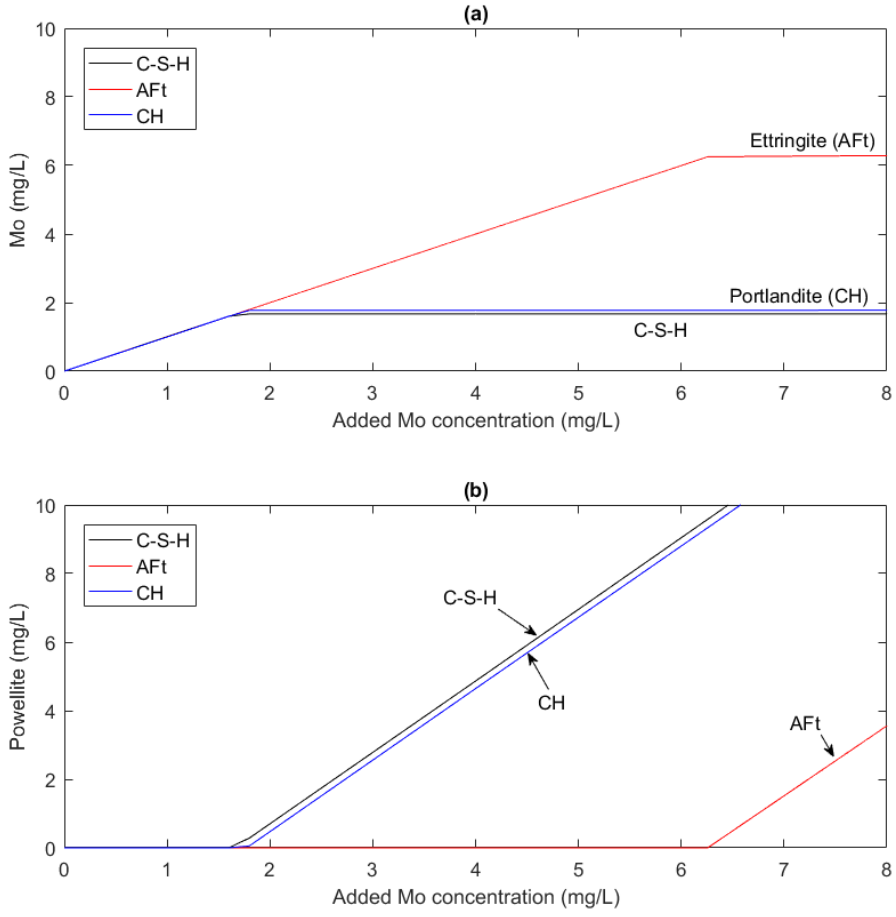

Figure 9 – Modeling of Mo concentrations in solution and the evolution of the precipitation of powellite at low initial Mo concentrations. All concentrations are given in mg/L of solution and plotted as function of the added Mo concentration.

5. Conclusion

The aims of this study were to: (i) compare the capacity of three cementitious binders to immobilize Mo in a single-step batch procedure, (ii) study the immobilization of Mo by the calcium silicate hydrate (C-S-H) phase, and (iii) contribute to the understanding of the mechanisms leading to Mo stabilization by comparing experimental data with thermodynamic models. To this end, three different binders were studied: one Ordinary Portland cement (OPC), one experimental binder composed of 90% ground granulated blast furnace slag (GGBS) and 10% OPC (90-10), and one supersulfated GGBS cement (SSC). All the binders were spiked with sodium molybdate using different Mo concentrations from 0.005 wt% to 10 wt% (% by weight of anhydrous binder) (50 to 10000 mg_{Mo}/kg_{binder}). In a second step, the syntheses of C-S-H in contact with Mo was also studied for Mo concentrations from 0.25 wt% to 5 wt%.

The main conclusions drawn from this study are:

1. Mo was strongly immobilized by the three binders studied (>74%). Supersulfated GGBS binder (SSC) showed the highest capacity to immobilize Mo over the range of Mo concentrations studied. The OPC and SSC binders allowed for the transition of Mo-spiked binders from “hazardous” to “non-inert and non-hazardous” waste category.
2. Powellite ($CaMoO_4$) precipitation was identified as the main mechanism of Mo stabilization. Powellite was detected by XRD analyses at high Mo concentrations, and thermodynamic calculations showed that all leaching solutions were slightly oversaturated with powellite.
3. In synthetic C-S-H, Mo stabilization was mainly controlled by the coprecipitation of powellite, and it was observed that the structure of C-S-H was not modified by the presence of Mo, so Mo uptake into the mineral lattice was excluded. However, the

stabilization of Mo at low concentrations by adsorption onto the C-S-H surface cannot be rejected.

4. Thermodynamic modeling showed that powellite formed at Mo concentrations higher than 1.7 mg/L ($1.7x10^{-5}$ mol/L) when the solution was saturated with respect to C-S-H or portlandite. In contrast, when the solution was saturated with respect to ettringite, powellite precipitated at Mo concentrations higher than 6.5 mg/L ($7x10^{-5}$ mol/L). At lower Mo concentrations, especially in ettringite containing binders, other stabilization mechanisms, such as substitution and adsorption, might be relevant.

The present study highlights the potential of alternative cementitious binders to efficiently immobilize Mo. However, the study was limited to model systems so that there is a need for further data on more complex real-world applications (e.g. Mo-contaminated soils or waste material). Under these conditions, there might be additional effects due to the presence of organic matter, ion competition and other reactive surfaces.

Credit authorship contribution statement

Laura Diaz Caselles: Investigation, Methodology, Writing – Original Draft, Project administration. **Cédric Roosz:** Software, Methodology, Writing – review and editing. **Julie Hot:** Supervision, Writing – review and editing. **Simon Blotevogel:** Conceptualization, Validation, Writing – review and editing. **Martin Cyr:** Conceptualization, Writing – review and editing, Supervision, Funding acquisition, Project administration.

Declaration of competing interest

The authors declare no conflict of interest.

Acknowledgments

685 This work was financially supported by the French Ministry of Higher Education and
686 Research and the National Association for Research and Technology (ANRT) in the
687 framework of French Cifre fellowships. Simon Blotevogel would recieved funding from the
688 EU by the Research Fund for Coal and Steel under grant agreement No 749809.

689 **References**

690 Basta, N.T., Ryan, J.A., Chaney, R.L., 2005. Trace element chemistry in residual-treated
691 soil: Key concepts and metal bioavailability. Journal of Environmental Quality 34, 49–
692 63. https://doi.org/10.2134/jeq2005.0049dup

693 Batchelor, B., 2006. Overview of waste stabilization with cement. Waste Management 26,
694 689–698. https://doi.org/10.1016/j.wasman.2006.01.020

695 Beganskienė, A., Sirutkaitis, V., Kurtinaitienė, M., Juškėnas, R., Kareiva, A., 2004. FTIR,
696 TEM and NMR investigations of Stöber silica nanoparticles. Mater Sci (Medžiagotyra)
697 10, 287–290.

698 Berger, S., 2009. Etude des potentialités des ciments sulfo-alumineux bélitique pour le
699 conditionnement du zinc : de l'hydratation à la durabilité. Université de Lille 1.

700 Blanc, P., Lassin, A., Piantone, P., Azaroual, M., Jacquemet, N., Fabbri, A., Gaucher, E.C.,
701 2012. Thermoddem: A geochemical database focused on low temperature water/rock
702 interactions and waste materials. Applied Geochemistry 27, 2107–2116.
703 https://doi.org/10.1016/j.apgeochem.2012.06.002

704 Blotevogel, S., Ehrenberg, A., Steger, L., Doussang, L., Kaknics, J., Patapy, C., Cyr, M.,
705 2020. Ability of the R3 test to evaluate differences in early age reactivity of 16 industrial
706 ground granulated blast furnace slags (GGBS). Cement and Concrete Research 130,
707 105998. https://doi.org/10.1016/j.cemconres.2020.105998

708 Bourg, A.C.M., Loch, J.P.G., 1995. Mobilization of Heavy Metals as Affected by pH and

709 Redox Conditions, in: Biogeodynamics of Pollutants in Soils and Sediments. Springer
710 Berlin Heidelberg, Berlin, Heidelberg, pp. 87–102. https://doi.org/10.1007/978-3-642-
711 79418-6_4

712 Brown, P.W., Bothe, J. V., 1993. The stability of ettringite. Advances in Cement Research 5,
713 47–63. https://doi.org/10.1680/adcr.1993.5.18.47

714 Buj, I., Torras, J., Rovira, M., de Pablo, J., 2010. Leaching behaviour of magnesium
715 phosphate cements containing high quantities of heavy metals. Journal of Hazardous
716 Materials 175, 789–794. https://doi.org/10.1016/j.jhazmat.2009.10.077

717 Cabrerizo, A., Bulteel, D., Waligora, J., Landrot, G., Fonda, E., Olard, F., 2020. Chemical,
718 mineralogical, and environmental characterization of tunnel boring muds for their
719 valorization in road construction: a focus on molybdenum characterization.
720 Environmental Science and Pollution Research. https://doi.org/10.1007/s11356-020-
721 09969-6

722 Chen, L., Wang, Y.-S., Wang, L., Zhang, Y., Li, J., Tong, L., Hu, Q., Dai, J.-G., Tsang,
723 D.C.W., 2021. Stabilisation/solidification of municipal solid waste incineration fly ash by
724 phosphate-enhanced calcium aluminate cement. Journal of Hazardous Materials 408,
725 124404. https://doi.org/10.1016/j.jhazmat.2020.124404

726 Chen, Q.Y., Tyrer, M., Hills, C.D., Yang, X.M., Carey, P., 2009. Immobilisation of heavy
727 metal in cement-based solidification/stabilisation: A review. Waste Management 29,
728 390–403. https://doi.org/10.1016/j.wasman.2008.01.019

729 Chen, W., Brouwers, H.J.H., 2007. The hydration of slag, part 2: Reaction models for
730 blended cement. Journal of Materials Science 42, 444–464.
731 https://doi.org/10.1007/s10853-006-0874-1

732 Chrysochoou, M., Dermatas, D., 2006. Evaluation of ettringite and hydrocalumite formation

733 for heavy metal immobilization: Literature review and experimental study. Journal of
734 Hazardous Materials 136, 20–33. https://doi.org/10.1016/j.jhazmat.2005.11.008

735 Diaz Caselles, L., Hot, J., Roosz, C., Cyr, M., 2020. Stabilization of soils containing sulfates
736 by using alternative hydraulic binders. Applied Geochemistry 113, 104494.
737 https://doi.org/10.1016/j.apgeochem.2019.104494

738 Diotti, A., Perèz Galvin, A., Piccinali, A., Plizzari, G., Sorlini, S., 2020. Chemical and
739 Leaching Behavior of Construction and Demolition Wastes and Recycled Aggregates.
740 Sustainability 12, 10326. https://doi.org/10.3390/su122410326

741 Erdman, J.A., Ebens, R.J., Case, A.A., 1978. Molybdenosis: A Potential Problem in
742 Ruminants Grazing on Coal Mine Spoils. Journal of Range Management 31, 34.
743 https://doi.org/10.2307/3897628

744 Essington, M.E., 1990. Calcium molybdate solubility in spent oil shale and a preliminary
745 evaluation of the association constants for the formation of CaMoO40(aq), KMoO4-(aq),
746 and NaMoO4-(aq). Environmental Science & Technology 24, 214–220.
747 https://doi.org/10.1021/es00072a010

748 Felmy, A.R., Rai, D., Mason, M.J., 1992. The solubility of CaMoO4(c) and an aqueous
749 thermodynamic model for Ca2+-MoO 4 2 -ion-interactions. Journal of Solution
750 Chemistry 21, 525–532. https://doi.org/10.1007/BF00649561

751 Gaboreau, S., Grangeon, S., Claret, F., Ihiawakrim, D., Ersen, O., Montouillout, V., Maubec,
752 N., Roosz, C., Henocq, P., Carteret, C., 2020. Hydration Properties and Interlayer
753 Organization in Synthetic C-S-H. Langmuir 36, 9449–9464.
754 https://doi.org/10.1021/acs.langmuir.0c01335

755 Glasser, F.P., 2004. The stability of ettringite, in: International RILEM Workshop on Internal
756 Sulfate Attack and Delayed Ettringite Formation. RILEM Publications SARL, pp. 43–64.

https://doi.org/10.1617/2912143802.004

Glasser, F.P., 1997. Fundamental aspects of cement solidification and stabilisation. Journal of Hazardous Materials 52, 151–170. https://doi.org/10.1016/S0304-3894(96)01805-5

Goetz-Neunhoeffer, F., Neubauer, J., 2006. Refined ettringite (Ca6Al2(SO4)3(OH)12 ·26H2O) structure for quantitative X-ray diffraction analysis. Powder Diffraction 21, 4–11. https://doi.org/10.1154/1.2146207

Goldberg, S., 2006. Geochemistry, Groundwater and Pollution. Vadose Zone Journal 5, 510–510. https://doi.org/10.2136/vzj2005.1110br

Goldberg, S., Forster, H.S., Godfrey, C.L., 1996. Molybdenum Adsorption on Oxides, Clay Minerals, and Soils. Soil Science Society of America Journal 60, 425–432. https://doi.org/10.2136/sssaj1996.03615995006000020013x

Grambow, B., López-García, M., Olmeda, J., Grivé, M., Marty, N.C.M., Grangeon, S., Claret, F., Lange, S., Deissmann, G., Klinkenberg, M., Bosbach, D., Bucur, C., Florea, I., Dobrin, R., Isaacs, M., Read, D., Kittnerová, J., Drtinová, B., Vopálka, D., Cevirim-Papaioannou, N., Ait-Mouheb, N., Gaona, X., Altmaier, M., Nedyalkova, L., Lothenbach, B., Tits, J., Landesman, C., Rasamimanana, S., Ribet, S., 2020. Retention and diffusion of radioactive and toxic species on cementitious systems: Main outcome of the CEBAMA project. Applied Geochemistry 112. https://doi.org/10.1016/j.apgeochem.2019.104480

Guo, B., Liu, B., Yang, J., Zhang, S., 2017. The mechanisms of heavy metal immobilization by cementitious material treatments and thermal treatments: A review. Journal of Environmental Management 193, 410–422. https://doi.org/10.1016/j.jenvman.2017.02.026

Gupta, U.C., 1997. Molybdenum in agriculture, Choice Reviews Online. Cambridge

University Press. https://doi.org/10.5860/CHOICE.35-0287

Gustafsson, J.P., Tiberg, C., 2015. Molybdenum binding to soil constituents in acid soils: An XAS and modelling study. Chemical Geology 417, 279–288. https://doi.org/10.1016/j.chemgeo.2015.10.016

Helgeson, H.C., 1969. Thermodynamics of hydrothermal systems at elevated temperatures and pressures. American Journal of Science 267, 729–804. https://doi.org/10.2475/ajs.267.7.729

Helser, J., Cappuyns, V., 2021. Trace elements leaching from Pb[sbnd]Zn mine waste (Plombières, Belgium) and environmental implications. Journal of Geochemical Exploration 220. https://doi.org/10.1016/j.gexplo.2020.106659

Hewlett, P.C., Liska, M. (Eds.), 2019. Lea's Chemistry of Cement and Concrete, Science. Elsevier. https://doi.org/10.1016/C2013-0-19325-7

Hills, C.D., Sollars, C.J., Perry, R., 1994. A calorimetric and microstructural study of solidified toxic wastes -Part 2: A model for poisoning of OPC hydration. Waste Management 14, 601–612. https://doi.org/10.1016/0956-053X(94)90032-9

Kindness, A., Lachowski, E.E., Minocha, A.K., Glasser, F.P., 1994. Immobilisation and fixation of molybdenum (VI) by Portland cement. Waste Management 14, 97–102. https://doi.org/10.1016/0956-053X(94)90002-7

Kogbara, R.B., Al-Tabbaa, A., 2011. Mechanical and leaching behaviour of slag-cement and lime-activated slag stabilised/solidified contaminated soil. Science of the Total Environment 409, 2325–2335. https://doi.org/10.1016/j.scitotenv.2011.02.037

Kolani, B., Buffo-Lacarrière, L., Sellier, A., Escadeillas, G., Boutillon, L., Linger, L., 2012. Hydration of slag-blended cements. Cement and Concrete Composites 34, 1009–1018. https://doi.org/10.1016/j.cemconcomp.2012.05.007

Lange, S., Klinkenberg, M., Barthel, J., Bosbach, D., Deissmann, G., 2020. Uptake and retention of molybdenum in cementitious systems. Applied Geochemistry 119, 104630. https://doi.org/10.1016/j.apgeochem.2020.104630

Legifrance, 2014. Arrêté du 12 décembre 2014 relatif aux conditions d'admission des déchets inertes dans les installations relevant des rubriques 2515, 2516, 2517 et dans les installations de stockage de déchets inertes relevant de la rubrique 2760 de la nomenclature des i. France.

Li, J., Chen, L., Zhan, B., Wang, L., Poon, C.S., Tsang, D.C.W., 2021. Sustainable stabilization/solidification of arsenic-containing soil by blast slag and cement blends. Chemosphere 271, 129868. https://doi.org/10.1016/j.chemosphere.2021.129868

Mancini, G., Palmeri, F., Luciano, A., Viotti, P., Fino, D., 2020. Partial Stabilization of Mo-Containing Hazardous Wastes Using a Ferrous Sulfate-Based Additive as a Redox Agent. Waste and Biomass Valorization. https://doi.org/10.1007/s12649-020-01095-1

Marks, J.A., Perakis, S.S., King, E.K., Pett-Ridge, J., 2015. Soil organic matter regulates molybdenum storage and mobility in forests. Biogeochemistry 125, 167–183. https://doi.org/10.1007/s10533-015-0121-4

Marty, N.C.M., Grangeon, S., Elkaïm, E., Tournassat, C., Fauchet, C., Claret, F., 2018. Thermodynamic and crystallographic model for anion uptake by hydrated calcium aluminate (AFm): An example of molybdenum. Scientific Reports 8, 1–13. https://doi.org/10.1038/s41598-018-26211-z

Matschei, T., Bellmann, F., Stark, J., 2005. Hydration behaviour of sulphate-activated slag cements. Advances in Cement Research 17, 167–178. https://doi.org/10.1680/adcr.2005.17.4.167

Minocha, A., Goyal, M.H., 2013. Immobilization of Molybdenum in Ordinary Portland

829 Cement. Journal of Chemical Engineering & Process Technology 04, 5–10.
830 https://doi.org/10.4172/2157-7048.1000162

831 Nikravan, M., Ramezanianpour, A.A., Maknoon, R., 2020. Study on physiochemical
832 properties and leaching behavior of residual ash fractions from a municipal solid waste
833 incinerator (MSWI) plant. Journal of Environmental Management 260, 110042.
834 https://doi.org/10.1016/j.jenvman.2019.110042

835 Park, C.K., 2000. Hydration and solidification of hazardous wastes containing heavy metals
836 using modified cementitious materials. Cement and Concrete Research 30, 429–435.
837 https://doi.org/10.1016/S0008-8846(99)00272-0

838 Parkhurst, D.L., Appelo, C.A.J., 2013. PHREEQC (Version 3)-A Computer Program for
839 Speciation, Batch-Reaction, One-Dimensional Transport, and Inverse Geochemical
840 Calculations, Modeling Techniques, book 6. https://doi.org/Rep. 99-4259

841 Plant, J., Smith, D., Smith, B., Williams, L., 2001. Environmental geochemistry at the global
842 scale. Applied Geochemistry 16, 1291–1308. https://doi.org/10.1016/S0883-
843 2927(01)00036-1

844 Ponta, O., Ciceo-Lucacel, R., Vulpoi, A., Radu, T., Simon, V., Simon, S., 2015. Synthesis
845 and characterisation of nanostructured silica-powellite-HAP composites. Journal of
846 Materials Science 50, 577–586. https://doi.org/10.1007/s10853-014-8615-3

847 Roosz, C., Gaboreau, S., Grangeon, S., Prêt, D., Montouillout, V., Maubec, N., Ory, S.,
848 Blanc, P., Vieillard, P., Henocq, P., 2016. Distribution of Water in Synthetic Calcium
849 Silicate Hydrates. Langmuir 32, 6794–6805.
850 https://doi.org/10.1021/acs.langmuir.6b00878

851 Scrivener, K., Snellings, R., Lothenbach, B., 2015. A Practical Guide to Microstructural
852 Analysis of Cementitious Materials.

853 Smedley, P.L., Kinniburgh, D.G., 2017. Molybdenum in natural waters: A review of
854 occurrence, distributions and controls. Applied Geochemistry 84, 387–432.
855 https://doi.org/10.1016/j.apgeochem.2017.05.008

856 Spence, R.D., Shi, C., 2004. Stabilization and solidification of hazardous, radioactive, and
857 mixed wastes, Stabilization and Solidification of Hazardous, Radioactive, and Mixed
858 Wastes. CRC Press. https://doi.org/10.1016/s0956-053x(97)88232-3

859 Taylor, H.F.W., 1997. Cement chemistry, 2nd editio. ed. Thomas Telford Publishing.
860 https://doi.org/10.1680/cc.25929

861 Van Gestel, C.A.M., McGrath, S.P., Smolders, E., Ortiz, M.D., Borgman, E., Verweij, R.A.,
862 Buekers, J., Oorts, K., 2012. Effect of long-term equilibration on the toxicity of
863 molybdenum to soil organisms. Environmental Pollution 162, 1–7.
864 https://doi.org/10.1016/j.envpol.2011.10.013

865 Vollpracht, A., Brameshuber, W., 2016. Binding and leaching of trace elements in Portland
866 cement pastes. Cement and Concrete Research 79, 76–92.
867 https://doi.org/10.1016/j.cemconres.2015.08.002

868 Wang, L., Cho, D.-W., Tsang, D.C.W., Cao, X., Hou, D., Shen, Z., Alessi, D.S., Ok, Y.S.,
869 Poon, C.S., 2019. Green remediation of As and Pb contaminated soil using cement-free
870 clay-based stabilization/solidification. Environment International 126, 336–345.
871 https://doi.org/10.1016/j.envint.2019.02.057

872 Wang, L., Geddes, D.A., Walkley, B., Provis, J.L., Mechtcherine, V., Tsang, D.C.W., 2020.
873 The role of zinc in metakaolin-based geopolymers. Cement and Concrete Research
874 136, 106194. https://doi.org/10.1016/j.cemconres.2020.106194

875 Wenzel, W.W., Alloway, B.J., 2013. Heavy Metals in Soils, 3rd ed, Heavy metals in Soils,
876 Environmental Pollution. Springer Netherlands, Dordrecht. https://doi.org/10.1007/978-

877 94-007-4470-7

878 Wichard, T., Mishra, B., Myneni, S.C.B., Bellenger, J.-P., Kraepiel, A.M.L., 2009. Storage
879 and bioavailability of molybdenum in soils increased by organic matter complexation.
880 Nature Geoscience 2, 625–629. https://doi.org/10.1038/ngeo589

881 World Health Organization, 2004. Guidelines for Drinking-water Quality. Geneva.
882 https://doi.org/ISBN 92 4 154638 7

883 Yang, P.-T., Wang, S.-L., 2021. Sorption and speciation of molybdate in soils: Implications
884 for molybdenum mobility and availability. Journal of Hazardous Materials 408, 124934.
885 https://doi.org/10.1016/j.jhazmat.2020.124934

886 Zhang, M., Reardon, E.J., 2003. Removal of B, Cr, Mo, and Se from Wastewater by
887 Incorporation into Hydrocalumite and Ettringite. Environmental Science & Technology
888 37, 2947–2952. https://doi.org/10.1021/es020969i

889 Zhu, C., Anderson, G., 2002. Environmental Applications of Geochemical Modeling.
890 Cambridge University Press. https://doi.org/10.1017/CBO9780511606274

891

Initial Mo concentrations (ppm)

100000
50000
10000
1000
500
100
50
10
1
0.1

Stabilization/solidification using cementitious binders and synthetic C-S-H

Mo immobilization by powellite ($CaMoO_4$) precipitation

○ Concentrations used for binder spike
△ Concentrations used for C-S-H syntheses

Final leached Mo concentrations (ppm)

100000
10000
1000
100
10
1
0.1

B2
B1
B3

C-S-H → Hazardous*

Non-inert and non-hazardous*

Inert and non-hazardous*

Binder	Mo retention in solid
B1: Ordinary Portland Cement	74 – 98%
B2: 90% GGBS and 10% OPC	32 – 94%
B3: Supersulfated GGBS cement	92 – 99%

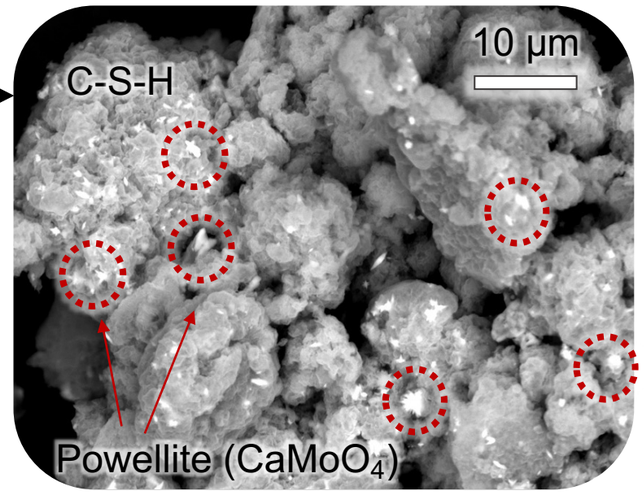

** Waste category: following the European definitions (Directive 2008/98/EC, decision 2000/532/EC and decision 2001/573/EC) adopted by the French Ministerial decree on waste classification for disposal.*